Helsinki University of Technology
Inorganic Chemistry Publication Series
Espoo 2006 No. 5

ATOMIC LAYER DEPOSITION OF HIGH-*k* DIELECTRICS FROM NOVEL CYCLOPENTADIENYL-TYPE PRECURSORS

Jaakko Niinistö

Dissertation for the degree of Doctor of Science in Technology to be presented with due permission of the Department of Chemical Technology for public examination and debate in Auditorium TU 1 at Helsinki University of Technology (Espoo, Finland) on the 12th of May, 2006, at 12 noon.

Helsinki University of Technology
Department of Chemical Technology
Laboratory of Inorganic and Analytical Chemistry

Teknillinen korkeakoulu
Kemian tekniikan osasto
Epäorgaanisen ja analyyttisen kemian laboratorio

Distribution:
Helsinki University of Technology
Laboratory of Inorganic and Analytical Chemistry
P.O. Box 6100
FIN-02150 TKK, FINLAND
E-mail: Jaakko.Niinisto@tkk.fi

ISBN 951-22-8169-4
ISSN 1458-5154

Otamedia Oy
Helsinki 2006

ABSTRACT

The atomic layer deposition (ALD) method was applied for fabricating high permittivity (high-*k*) dielectrics, *viz.* HfO_2, ZrO_2 and rare earth oxides, which can be used to replace SiO_2 as gate and capacitor dielectric. The dielectrics were processed by ALD using novel cyclopentadienyl (Cp, $-C_5H_5$) precursors together with water or ozone as the oxygen source. ALD, which has been identified as an important thin film growth technique for microelectronics manufacturing, relies on sequential and saturating surface reactions of alternately applied precursors, separated by inert gas purging. The surface-controlled nature of ALD enables the growth of thin films of high conformality and uniformity with an accurate thickness control.

The ALD technique is introduced and ALD processes for HfO_2, ZrO_2 and rare earth oxide films, as well as the applications of the high-*k* dielectrics in microelectronics are reviewed. The need for developing new ALD processes for the high-*k* materials is emphasized.

ALD processes for HfO_2 and ZrO_2 were developed using Cp-type precursors. The effect of different oxygen sources, namely water or ozone, on the film growth characteristics and properties of the ALD-processed films was examined in detail. The oxide films were stoichiometric, with impurity levels below even 0.1 at-% for C or H. Electrical measurements showed promising dielectric properties such as high permittivity values and low leakage current densities. Other properties, such as structure, interfacial layer thickness and morphology, were also characterized. Compared to films processed by water, the ozone-processed films on H-terminated Si showed improved dielectric properties, as well as higher density, lower roughness and better initial growth rate. In addition, *in situ* gas-phase measurements by quadrupole mass spectrometry (QMS) were performed in order to study the ZrO_2 growth mechanism.

A number of Cp-precursors were tested for the ALD of several rare earth oxide films. The thermal stability of many of the precursors was limited, but nevertheless, ALD-type processes were developed for Y_2O_3 and Er_2O_3 films. High reactivity of the Cp-precursors towards water resulting in high growth rates (1.2-1.7 Å/cycle) and purity of the Y_2O_3 and Er_2O_3 films were realized. Despite the detected partial decomposition of the $(CpMe)_3Gd$ precursor, Gd_2O_3 films with high growth rate and purity as well as effective permittivity of about 14 were deposited.

Finally, promising processes for ternary scandates, namely $YScO_3$, $GdScO_3$, and $ErScO_3$, were developed using either Cp- or β-diketonate-based processes. These as-deposited ternary films were amorphous exhibiting high effective permittivity (14-15), low leakage current density, and resistance towards crystallization upon annealing even up to 800°C.

PREFACE

The research reported in this thesis was carried out during the years 2001-2005 in the Laboratory of Inorganic and Analytical Chemistry (LIAC), Helsinki University of Technology.

I am most grateful to Dr. Matti Putkonen and Prof. Lauri Niinistö for the guidance and advice as well as for the initiative and possibility to carry out research on this interesting topic. My supervisor, Prof. Markku Leskelä as well as Prof. Mikko Ritala are thanked for invaluable help and the opportunity to use the research facilities at the Laboratory of Inorganic Chemistry, University of Helsinki.

I wish to thank all of my co-authors and co-workers from Helsinki University of Technology, University of Helsinki, Uppsala University, and Tokyo Institute of Technology. Especially, I would like to thank Dr. Kaupo Kukli for his assistance in the electrical measurements, Lic. Sci. (Tech.) Jani Päiväsaari and Dr. Chuck Dezelah for good collaboration and fruitful discussions, Mr. Pekka Hassinen for the ALD reactor maintenance, Dr. Timo Sajavaara and Dr. Kai Arstila for the TOF-ERD analysis, Dr. Antti Rahtu for instruction on the use of the *in situ* mass spectrometry system, Dr. Jun Lu, Prof. Hisao Yamauchi, and Prof. Maarit Karppinen for providing the HR-TEM measurements, and Prof. Pekka Hautojärvi for providing the facilities for the AFM measurements. The other members of the inorganic chemistry staff of LIAC are thanked as well. In addition, Dr. Chuck Dezelah is thanked for revising the language of this thesis.

Financial support from the Jenny and Antti Wihuri Foundation, Graduate School of Inorganic Materials Chemistry, The Finnish Foundation of Technology, the Academy of Finland and Acta Chemica Scandinavica is gratefully acknowledged.

Finally I wish to thank my family, especially my wife Sari for her continuous support.

Espoo, February 2006

Jaakko Niinistö

LIST OF PUBLICATIONS

In addition to the present review, this thesis includes the following publications (I-IX), which are referred to in the text by their corresponding Roman numerals. In addition, some still unpublished deposition studies of various rare earth oxide films are discussed.

I Putkonen, M., Niinistö, J., Kukli, K., Sajavaara, T., Karppinen, M., Yamauchi, H., and Niinistö, L., ZrO_2 thin films grown on silicon substrates by atomic layer deposition with $Cp_2Zr(CH_3)_2$ and water as precursors, *Chem. Vap. Deposition* **9** (2003) 207-212.

II Niinistö, J., Putkonen, M., Niinistö, L., Kukli, K., Ritala, M., and Leskelä, M., Structural and dielectric properties of thin ZrO_2 films on silicon grown by atomic layer deposition from cyclopentadienyl precursor, *J. Appl. Phys.* **95** (2004) 84-91.

III Niinistö, J., Rahtu, A., Putkonen, M., Ritala, M., Leskelä, M., and Niinistö, L., *In situ* quadrupole mass spectrometry study of atomic-layer deposition of ZrO_2 using $Cp_2Zr(CH_3)_2$ and water, *Langmuir* **21** (2005) 7321-7325.

IV Niinistö, J., Putkonen, M., Niinistö, L., Stoll, S.L., Kukli, K., Sajavaara, T., Ritala, M., and Leskelä, M., Controlled growth of HfO_2 thin films by atomic layer deposition from cyclopentadienyl-type precursor and water, *J. Mater. Chem.* **15** (2005) 2271-2275.

V Niinistö, J., Putkonen, M., Niinistö, L., Arstila, K., Sajavaara, J. Lu, T., Kukli, K., Ritala, M., and Leskelä, M., HfO_2 films grown by ALD using cyclopentadienyl-type precursors and H_2O or O_3 as oxygen source, *J. Electrochem. Soc.* **153** (2006) F39-F45.

VI Niinistö, J., Putkonen, M., and Niinistö, L., Processing of Y_2O_3 thin films by atomic layer deposition from cyclopentadienyl-type compounds and water as precursors, *Chem. Mater*. **16** (2004) 2953-2958.

VII Niinistö, J., Petrova, N., Putkonen, M., Sajavaara, T., Arstila, K., and Niinistö L., Gadolinium oxide thin films by atomic layer deposition, *J. Cryst. Growth* **285** (2005) 191-200.

VIII Päiväsaari, J., Niinistö, J., Arstila, K., Kukli, K., Putkonen, M., and Niinistö, L., High growth rate of erbium oxide thin films in atomic layer deposition from $(CpMe)_3Er$ and water precursors, *Chem. Vap. Deposition* **11** (2005) 415-419.

IX Myllymäki, P., Nieminen, M., Niinistö, J., Putkonen, M., Kukli, K., and Niinistö L., High-permittivity $YScO_3$ thin films by atomic layer deposition using two precursor approaches, *J. Mater. Chem.* **16** (2006) 563-567.

THE AUTHOR'S CONTRIBUTION

Publication I	The research plan for the experimental work was made together with Dr. Matti Putkonen. The author was responsible for carrying out a part of the film depositions, AFM and electrical measurements. The author had a minor role in writing the article.
Publication II	The author planned the research together with Dr. Matti Putkonen and did the experimental work except for precursor synthesis, TEM, XRR, GI-XRD and XPS analyses. The author interpreted the results and wrote the article.
Publication III	The research plan was made together with Dr. Antti Rahtu. The author carried out the experiments, except for the precursor synthesis, interpreted the results together with Dr. Antti Rahtu and wrote the article.
Publication IV	The author planned the research and did the experimental work except for a minor part of the depositions, precursor synthesis, XRR and TOF-ERD analysis. The author interpreted the results and wrote the article.
Publication V	The author planned the research and did the experimental work except for precursor synthesis, XRR, TEM and TOF-ERD analysis. The author interpreted the results and wrote the article.
Publication VI	The research plan for the experimental work was made together with Dr. Matti Putkonen. The author did the experimental work except for TOF-ERD analysis. The author interpreted the results and wrote the article.
Publication VII	The author planned the research and did the experimental work except for TOF-ERD analysis and minor part of the depositions. The author interpreted the results and wrote the article.

Publication VIII The author assisted in planning of the research. The author was responsible for the AFM studies and characterizing the electrical properties. The author had a minor role in writing the article.

Publication IX The author assisted in the planning of film growth experiments relating to electrical measurements. The author was responsible for the AFM studies and analyzing the electrical properties. The author had a minor role in interpretation of the results and writing the article.

LIST OF ABBREVIATIONS AND ACRONYMS

acac	acetylacetonate
AES	Auger Electron Spectroscopy
AFM	Atomic Force Microscope/Microscopy
ALD	Atomic Layer Deposition
ALE	Atomic Layer Epitaxy
amd	amidinate, $NC(CH_3)N$
CET	Capacitance Equivalent oxide Thickness
CMOS	Complementary Metal Oxide Semiconductor
Cp	Cyclopentadienyl, C_5H_5
CVD	Chemical Vapor Deposition
dmae	dimethylaminoethoxide, $(CH_3)_2N(C_2H_5O)$
DRAM	Dynamic Random Access Memory
EOT	Equivalent Oxide Thickness
Et	ethyl, $-C_2H_5$
GI	Grazing Incidence
HR	High-Resolution
IC	Integrated Circuit
IL	Interfacial Layer
^{i}Pr	isopropyl,$-CH(CH_3)_2$
Me	methyl, $-CH_3$
ML	Monolayer
mmp	1-methoxy-2-methyl-2-propanolate
MOSFET	Metal Oxide Semiconductor Field Effect Transistor
QMS	Quadrupole Mass Spectrometry
RE	Rare Earth
rms	root mean square
RTA	Rapid Thermal Annealing
SIMS	Secondary Ion Mass Spectroscopy
^{t}Bu	*tert*-butyl, $-CH(CH_3)_3$
TEM	Transmission Electron Microscopy
thd	2,2,6,6-tetramethyl-3,5-heptanedione, $C_{11}H_{20}O_2$
TOF-ERDA	Time-Of-Flight Elastic Recoil Detection Analysis
XPS	X-ray Photoelectron Spectroscopy
XRD	X-Ray Diffraction
XRF	X-Ray Fluorescence
XRR	X-Ray Reflectivity

CONTENTS

1. INTRODUCTION

Thin layers of material, *i.e.* thin films or overlayers, on supporting substrates are used in numerous applications in modern technology, from optics and optoelectronics to microelectronics and nanotechnology as well as protective coatings and in devices where functional properties, such as magnetic, catalytic, gas sensing or superconductive, are needed.

In microelectronics, continuous shrinking of devices is necessary to improve the performance, which sets challenging requirements for the integrated circuit (IC) fabrication. New materials and techniques are required and materials must be grown in the form of very thin films into deep trenches and other 3-D structures with good conformality. As requirements tighten, novel thin film deposition techniques are needed in many applications. Atomic layer deposition (ALD) technology, originally known as atomic layer epitaxy (ALE), was developed and patented in the 1970s[1] for thin film electroluminescence (TFEL) display fabrication, where high quality insulating and luminescent films on large area substrates were required. The current interest in ALD in the microelectronics industry stems from the unique characteristics that this method offers: ultrathin films can be deposited on a large substrate area with excellent conformality and with control of thickness and composition at nanometer level.[2] ALD has high potential for use as a tool in microelectronics for high permittivity (high-*k*) film growth for complementary metal oxide semiconductor (CMOS) devices and dynamic random access memory (DRAM) capacitors as well as for ferroelectrics, barrier materials, and conductors such as metal gates.[3,4]

High-*k* dielectrics have been extensively studied due to the fact that SiO_2, which is traditionally used as a gate oxide in metal-oxide semiconductor field effect transistors (MOSFETs), can no longer function as an effective gate insulator as higher capacitance density with decreased gate oxide thickness is required for near-future device generations.[3,5-7] The tunneling current through the SiO_2 gate oxide would otherwise degrade the device performance. The solution for this problem is to choose another material with higher permittivity than 3.9, which is characteristic for SiO_2. In fact, silicon oxynitride, SiO_xN_y has already been used to extend the use of silicon oxide-based gate dielectrics but a long-term alternative solution needs to be found. The leading candidates considered to replace silicon oxide-based gate dielectrics are the oxides, silicates, and

oxynitrides of hafnium and zirconium as well as also those of the rare earth (RE) elements.[8] ALD has already been a widely studied method for the growth of HfO_2 and ZrO_2.

As ALD is a chemical deposition method, the precursor chemistry has a decisive effect on the quality and properties of the deposited films.[9,10] The most commonly used Zr and Hf precursors, *viz.* the halides, have potential drawbacks such as chlorine contamination of the films[11] and generation of corrosive by-products during the ALD-processing. For these reasons, new precursor chemistry needs to be developed. Another factor in the precursor chemistry of oxide film growth is the selection of the oxygen source, which can strongly affect the resulting properties.[12] Water, which is a commonly used oxygen source, can be replaced, when needed, by a more aggressive oxidant, ozone.

The deposition of RE oxides has not been as widely studied by ALD as the growth of group 4 oxides (TiO_2, ZrO_2 and HfO_2). Prior to this study, only a few processes were reported and the potential of ALD-grown RE oxides has not yet been fully exploited.

The purpose of this work was to develop new processes for the ALD of HfO_2, ZrO_2, and the RE oxides by applying a novel group of ALD precursors, *viz*. the true organometallic cyclopentadienyl (Cp, -C_5H_5) precursors. The literature part of this thesis reviews the current status of the ALD of high-*k* oxides focusing on Hf, Zr and RE oxides. The experimental part describes the development of ZrO_2 and HfO_2 ALD-processes from Cp-precursors. In order to better understand the chemistry involved in the Cp-based oxide processes, reaction mechanism studies are also presented. The effects and suitability of ozone as the oxygen source for high-*k* film deposition is experimentally evaluated. In addition, ALD processes for various RE oxides, both binary and ternary, were developed and the suitability of Cp-precursors as well as a comparison with the β-diketonate-based processes is presented. The majority of the experimental results are reported in publications I-IX. However, the applicability of several Cp-type RE precursors, including La-, Pr-, and Gd-precursors are reported here for the first time. In addition, novel processes for $GdScO_3$ and $ErScO_3$ are briefly introduced.

1.1 Dielectric layers in microelectronics

The key component of the ICs, the MOSFET structure consists of source, drain, channel, gate and gate oxide (Figure 1). In order to keep in pace with the demands of the semiconductor industry, the IC performance should be continuously improved. One aspect of improving the device performance, *e.g*. to create more powerful computers, has been the exponential increase in the number of transistors on a silicon chip. This exponential increase is known as the Moore's law, predicted already some 40 years ago,[13] described that the number of transistors integrated on a chip would double approximately every 2 years. The semiconductor industry has up to now closely followed this prediction, which requires the dimensions of a MOSFET to continuously decrease. In 2004, the Intel Itanium® 2 integrated about 592 million transistors, which is some 200 times more than in 1993 when the Intel Pentium® processor was introduced.[14] To obtain this scaling, the gate oxide layer, nitrided SiO_2 has been downscaled to as thin as 1.2 nm, or to a thickness of only a few monolayers. This thickness is already at a level where severe problems occur, and as a result the dielectric is not able to effectively withstand voltages, as tunneling current through the dielectric is detrimental on device performance. Another problem related to the SiO_2 scaling is reliability; the requirements for reliability are even more difficult to meet than the leakage current requirements.[8]

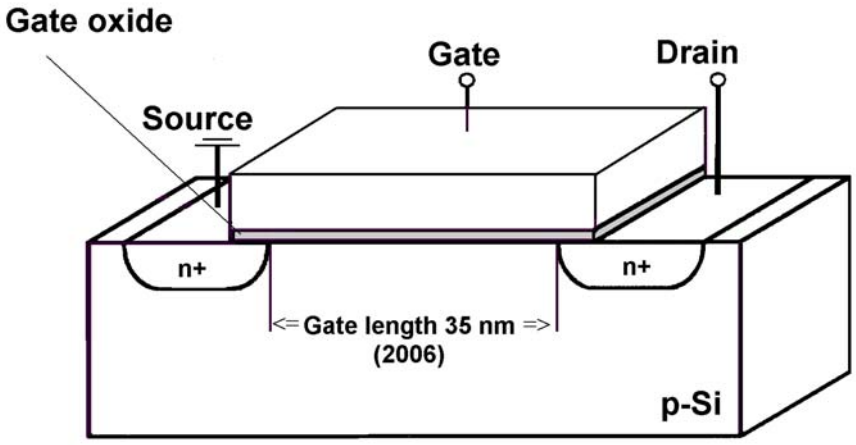

Figure 1. A Schematic showing a MOSFET structure.

The solution for the aforementioned problems related to SiO_2 scaling is to select a gate dielectric with a higher permittivity than that of SiO_2 (k = 3.9). The capacitance density (C/A) is directly proportional to permittivity:

$$\frac{C}{A} = \frac{\varepsilon_0 \varepsilon_r}{t_{ox}} \tag{1}$$

where ε_0 is the permittivity of the free space, ε_r permittivity (also referred to as relative dielectric constant), A the capacitor area, and t_{ox} the gate oxide thickness. It should be noted that the permittivity is also represented by the Greek letter κ, thus the expression high-κ or, as used in the current text, high-k are equivalent terms. The equation (1) can be rewritten in terms of EOT (equivalent oxide thickness) and the permittivity of SiO_2 (k = 3.9):

$$\mathrm{EOT} = \frac{t_{ox} 3.9}{\varepsilon_r (\text{high-}k)} \tag{2}$$

The term EOT thus represents the theoretical thickness of SiO_2 that would be needed to achieve the same capacitance density as with the high-k dielectric, *e.g.* if high-k material with a permittivity value four times higher than that of SiO_2 is used as gate dielectric, a 4 nm thick layer would have the same capacitance as a 1 nm thick SiO_2 layer; thus the EOT is 1 nm. It should be noted here, however, that if the equivalent thickness is determined solely from the accumulation capacitance and quantum mechanical effects are not taken into an account, another term CET (capacitance equivalent oxide thickness) is used, which yields slightly higher values than the EOT. Usually, the gate dielectric consists of several layers, *e.g.* a lower k interfacial layer (or layers) and higher k layer. In terms of EOT (or CET) the series capacitance can be written:

$$\mathrm{EOT}_{\mathrm{total}} = \mathrm{EOT}_{\text{high-}k} + \Sigma \mathrm{EOT}_{\text{low-}k} \tag{3}$$

Any low-k interfacial layer contributes to the overall EOT value and thus should be minimized in order to achieve the low enough EOT required.

Possessing sufficient permittivity is not the only condition an alternative high-k candidate must meet, actually the requirements are numerous, out of which five can be considered as the major requirements. First of all, as mentioned, for a longer term solution the permittivity of the material should be considerably higher than 3.9, preferably higher than

12.[7] This requirement excludes some candidates, such as Al_2O_3, which has a permittivity value of 9. Then, the metal oxide has to be thermally (up to 1000°C) and chemically stable in contact with Si in order to prevent reactions with Si leading to formation of thick interfacial SiO_x or silicide layers.[8,15,16] This requirement eliminates a number of potential high-*k* oxides, *e.g.* TiO_2, Ta_2O_5 and Nb_2O_5.[15,17] In addition, the candidate material is required to have high enough bandgap (>5 eV) to reduce the leakage current flowing through the structure.[7] Also the conduction band offset, in other words the barrier for electrons travelling from the silicon substrate to the gate, has to be sufficient (>1 eV).[7,17] If this value is low, high leakage currents may result, precluding the use of some materials (*e.g.* TiO_2 and Ta_2O_5) as alternative gate oxides. The low density of defects at the Si/dielectric interfacial region is also a challenging requirement.[8] An amorphous microstructure of the candidate material, even after post-deposition annealing, is most desirable, because a polycrystalline structure offers pathways for leakage current along grain boundaries. Epitaxial oxides would be a good solution, but they are difficult to grow on silicon.[18] Other important requirements include reliability,[19] as well as gate and process compatibility issues.[20]

Identifying the most promising high-*k* candidate is a demanding task. The requirements mentioned above limit the gate dielectric candidates to only a few (Table 1), among which the oxides of Zr and Hf are probably the most promising. The rare earth oxides can also be counted as potentially promising candidates, despite the fact that in some cases the permittivity increase is only moderate. Quite recently, amorphous ternary rare earth scandates have also been introduced as high-*k* candidates, *e.g.* $GdScO_3$ has been reported to have permittivity value of about 20,[21] which is considerably higher than those of the constituent oxides, Gd_2O_3 and Sc_2O_3. Besides the materials listed in Table 1, there are also other technical solutions of hafnium-based silicates and oxynitrides and some combinations of them such as HfSiON,[22] which has recently gained considerable interest. In addition to the silicates, aluminates have also been studied. However, their drawback, similarly as in the case of silicates, is the decreased permittivity due to the mixing of Al_2O_3 which has a lower permittivity than that of HfO_2. Unfortunately, aluminates have higher density of defects than the silicates.[17] Generally, the purpose for adding silicon, nitrogen or aluminum is to extend the crystallization onset temperature.

Table 1. Examples of high-*k* candidates as alternative gate or capacitor dielectrics.

Material	Permittivity	Material	Permittivity
Si_3N_4	7[5,8]	La_2O_3	20-30[5,8]
Al_2O_3	9[5,8]	PrO_x	30[23]
ZrO_2	14-25[8]	Gd_2O_3	9-14[8]
HfO_2	15-26[8]	Other Ln_2O_3 (Ln=Nd, Sm, Dy, Ho, Er, Yb, Lu)	9-14[8,24]
Y_2O_3	12-15[5,8]	$REScO_3$	20-22[21]

High-*k* materials are needed for memory applications as well. A DRAM stores each bit in a storage cell consisting of a capacitor and a transistor. Capacitors tend to quickly loose their charge and must be repeatedly recharged. The charge storage capacity of a capacitor is dependent on the capacitance. The capacitance can be increased by decreasing the SiO_2 dielectric thickness, increasing the surface area, and/or introducing a high-*k* dielectric. Storage capacitors can be divided in two types, stacked-capacitors and trench capacitors, of which the latter offers highest density, but the manufacturing process complexity can be considered as a drawback.[25] Figure 2 shows a schematic view of current DRAM architectures. The stacked-capacitors have now been introduced into the sub-100 nm technology CMOS nodes and the metal-insulator-metal capacitors where high-*k* materials, such as Ta_2O_5, are applied.[3] However, potential long-term solutions are based on ultrahigh-*k* dielectrics, such as perovskites. In trench capacitor structures (Figure 2) the capacitors are constructed into high aspect ratio trenches in order to increase the surface area and thus the effective capacitance density. The area can further be increased by widening the trench profile (bottle-shape trenches) and by roughening the sidewalls of the trenches.[3] A near-future solution for insulator in trench capacitor structures is similar as in the case of gate dielectric applications where Hf-based materials and in addition Al_2O_3 have been applied. As the trench aspect ratio is expected to increase up to 80:1 by the year 2007, ALD is probably the only viable technique for such depositions.[3]

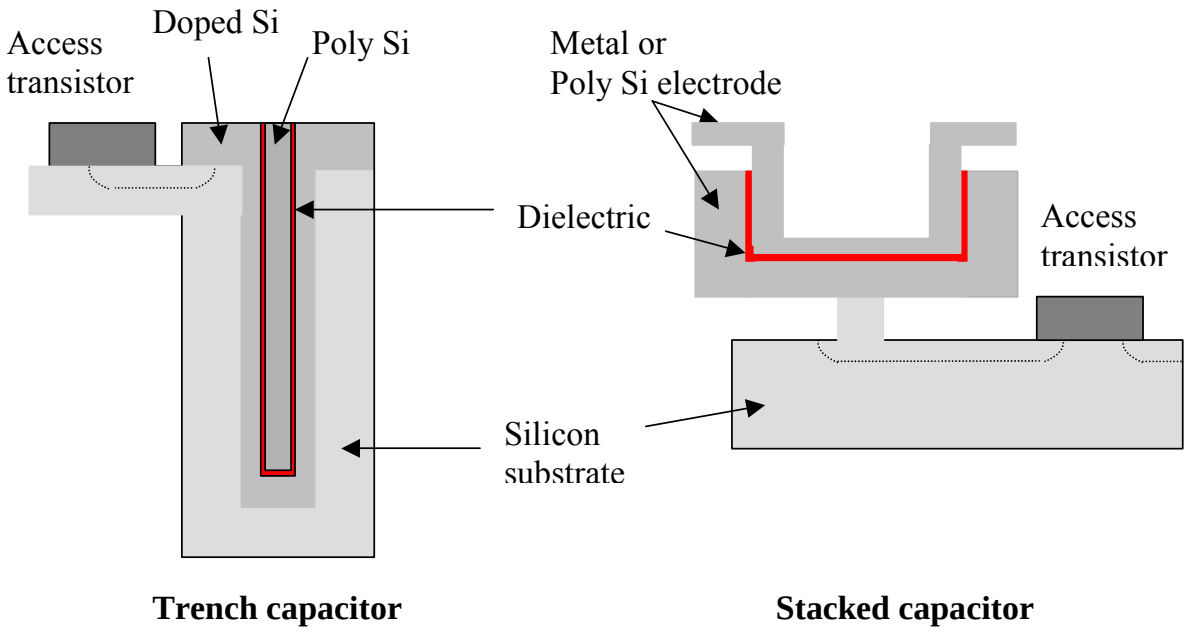

Figure 2. A schematic showing two types of DRAM capacitor structures: trench and stack architecture.

1.2 Atomic layer deposition

As briefly described earlier, the ALD technology was developed and patented some 30 years ago by Suntola and co-workers in Finland.[1] The purpose was to develop TFEL displays where ALD, then known as ALE, was used to deposit the high quality electroluminescent and dielectric layers, the latter being closely related to the high-*k* dielectrics. The TFEL display production was the first industrial application of ALD and the successful industrial production still continues.[26] The strength of the ALD technology lies in its capability to produce high-quality, dense, and pinhole-free films on large surface areas with excellent uniformity and conformality as well as with thickness and composition control at an atomic level.[2,9] These characteristics are now especially needed for the processing of high-*k* dielectrics.

The ALD processes and their applications have been frequently reviewed,[2,12,27-29] most extensively and recently by Puurunen[30] as well as by Ritala and Leskelä.[9] ALD is a variant of chemical vapor deposition (CVD) method, but unlike CVD, ALD relies on sequential and saturating surface reactions of the alternately applied precursor pulses. The precursor

pulses are separated by inert gas purging or evacuation of the reaction chamber to avoid gas phase reactions between the precursors. The growth proceeds in a cyclic manner enabling easy thickness control. The basic principle of ALD is shown in a simplified manner in Figure 3, where one ALD cycle of an imaginary metal oxide deposition is presented. At first the exposure of the substrate surface to the gaseous metal precursor (a) and its chemisorption on the available surface sites (here –OH groups) leaves the surface saturated. After inert gas purging of the excess precursor and ligand exchange by-products (b), the surface is exposed to the oxygen source (here H_2O) (c). The surface reaction produces the desired oxide film and after inert gas purging the surface is ready for the next ALD cycle (d).

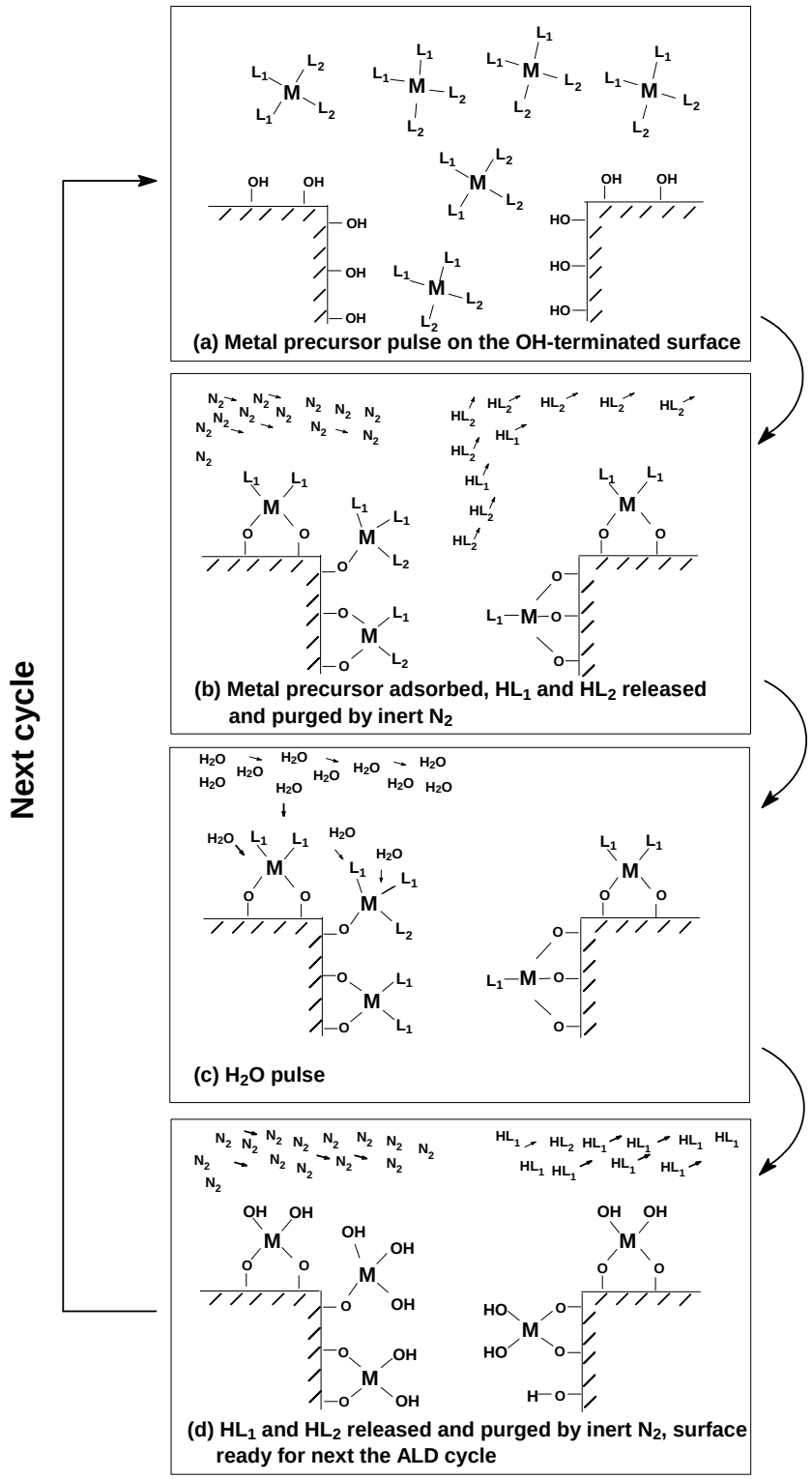

Figure 3. Schematic illustration of an ALD cycle of a hypothetical metal oxide process where precursors, L_1ML_2 (M=metal, $L_{1,2}$=ligands, *e.g.* CH_3, Cl, Cp, alkylamide) and H_2O are alternately pulsed and separated by inert gas pulsing. Instead of inert gas pulsing evacuation of the reaction chamber can be used.

In order to achieve a surface saturative ALD-type process, the growth rate has to be independent of the precursor dose provided that the dose is sufficiently large so that all the available surface sites have been occupied (Figure 4a). In other words, the precursor decomposition leading to a CVD-type growth mode should be avoided. In theory, the ALD growth proceeds by one atomic layer per cycle, but in practice, due to steric hindrances and possible limited number of reactive surface sites, the growth rate per cycle usually is only a distinct fraction of a monolayer (ML) thickness, typically less than 0.5 ML. As the growth proceeds in a cyclic manner, and the purging periods take some time, the ALD technique is rather slow for some applications, but for high-*k* depositions where very thin films are grown this is not a critical issue.

Often, but not always, a region with a constant deposition rate, also known as ALD window, is observed.[12,31] The ALD window is not a requirement for an ALD-type growth mode, but it is a desirable feature that leads to the reproducibility of the film growth. Especially if a ternary material is to be deposited, overlapping ALD windows of the constituent binary processes offer a good starting point for the development of a ternary process. The observed growth rates *vs.* temperature in ALD processes are shown in Figure 4b.

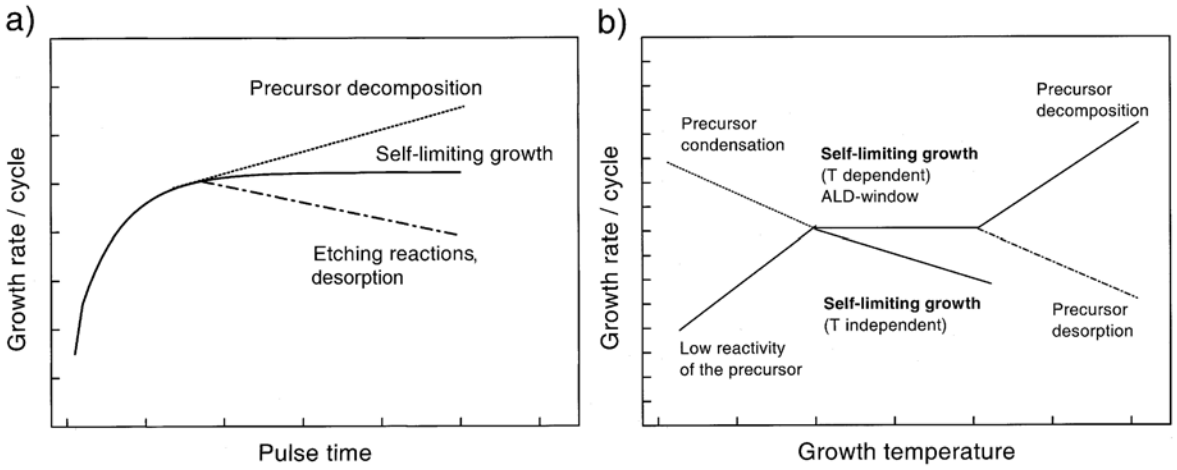

Figure 4. Different types of growth rate *vs.* precursor pulse time curves in ALD processes at a constant temperature (a) and factors limiting the self-limiting growth at various temperatures (b).

In addition to the above-mentioned applications in microelectronics, ALD certainly offers potential solutions in many other areas, such as optics and optoelectronics, nanotechnology, micro-electromechanical systems, catalysis, magnetic recording head technology, and protective and antireflective coatings.[9]

1.3 Precursor chemistry in ALD of oxide films

Besides having an efficient reactor with uniform gas distribution within the reaction space,[32] careful selection of the precursor is of an utmost importance for a successful ALD process. The main requirements for a good ALD precursor can be listed as follows. The precursor must be sufficiently volatile and must not undergo significant self-decomposition at deposition temperature, a problem which leads to a CVD-type growth mode. The precursor must adsorb or react with the surface sites, and its reactivity must be sufficient also towards the oxygen source. In contrast to CVD, the ΔG value for the reaction should be as negative as possible.[9] Furthermore, the precursor and its reaction by-products should not etch the surface or the growing film. Important factors include also practical aspects, such as safety and economical requirements.[9,12] In addition, liquid or gaseous precursors are generally preferred over the solid ones.

1.3.1 Metal precursor types

The various metal precursor types applied in ALD of oxide films are schematically presented in Figure 5. Here, the metal precursor types are introduced only briefly; more detailed examples of the precursors used for high-*k* materials will be presented in Section 1.4.

The most common group of inorganic precursors in ALD are the halides, where the metal atom is bonded to halogen atoms (F, Cl, Br or I). For example, $HfCl_4$ together with water is one the most frequently studied ALD process and will be discussed in more detail in Section 1.4.2. The beneficial characteristics of many metal halides include their high thermal stability over a wide temperature range, good reactivity and wide availability as volatile compounds for many metals. Furthermore, they are readily available and/or can be easily synthesized. However, drawbacks include possible generation of particles and corrosive by-products as well as halide contamination in the deposited films. Other purely

inorganic precursors are occasionally used despite their limited stability, for instance, the metal nitrates.[33]

Alkoxides, where the metal ion is bonded to the oxygen, have been frequently applied for the ALD of various oxide films. However, thermal stability of the alkoxides is limited and ALD-type growth mode is not often achieved.[34,35,36] The β-diketonates, used frequently in CVD,[37-39] have also been studied for the ALD of RE oxide films.[40,24] Because the C-O bond is relatively strong, powerful oxidizers are needed, but still, some carbon is left in the film.[24] In addition, steric hindrance, caused by the bulky size of the ligands results in low growth rates. It should be noted, though, that for the rare earth oxides not many other types of viable precursors exist and thus the β-diketonates form an important group of precursors in ALD of RE oxides.[24]

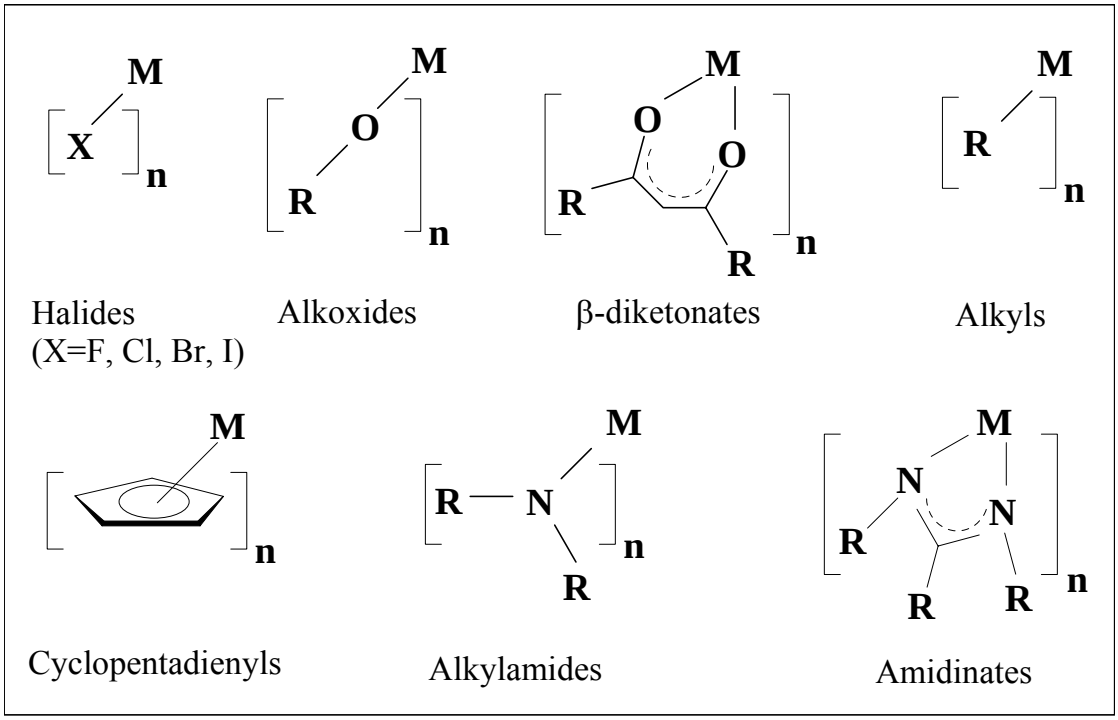

Figure 5. Examples of precursor types applied in the ALD of oxide thin films. The R's represent alkyl groups such as methyl (Me) or ethyl (Et).

Among the precursors where the metal is bonded to nitrogen, dialkylamido (alkylamides) and amidinato complexes have recently gained attention.[10,41] Alkyl amides are volatile and reactive towards water, which makes the group interesting as precursors for high-*k*

materials. However, as described in Section 1.4.1 the thermal stability can be a problem in some cases. The self-decomposition of the precursor seems to be affecting the growth characteristics also in the case of amidinates.[42]

The true organometallics, *viz.* the metal alkyls and cyclopentadienyl compounds, can be exploited in ALD for high quality film growth. For example, $AlMe_3/H_2O$ is an excellent ALD process for the deposition of Al_2O_3.[30] Alkyls are highly volatile and reactive but their availability is rather limited and presently they are used as precursors for Al and Zn containing films.[30,43] Cyclopentadienyl or metallocene compounds, having at least one direct metal-carbon bond to the Cp-ligand (C_5H_5), offer a wider range of possibilities as precursors. The Cp-compounds, first synthesized in the 1950s,[44,45] are generally volatile and highly reactive, and thus suitable as ALD precursors.[46] Cp-compounds have been previously applied for various ALD processes (see the recent review by Putkonen and Niinistö[46]), but not extensively for high-*k* gate oxide depositions. They have also been applied as catalysts,[47] and thus the commercial availability in many cases is good. Often, however, thermal stability is limited, but a wide variety of different substituents exists as seen in Figure 6.

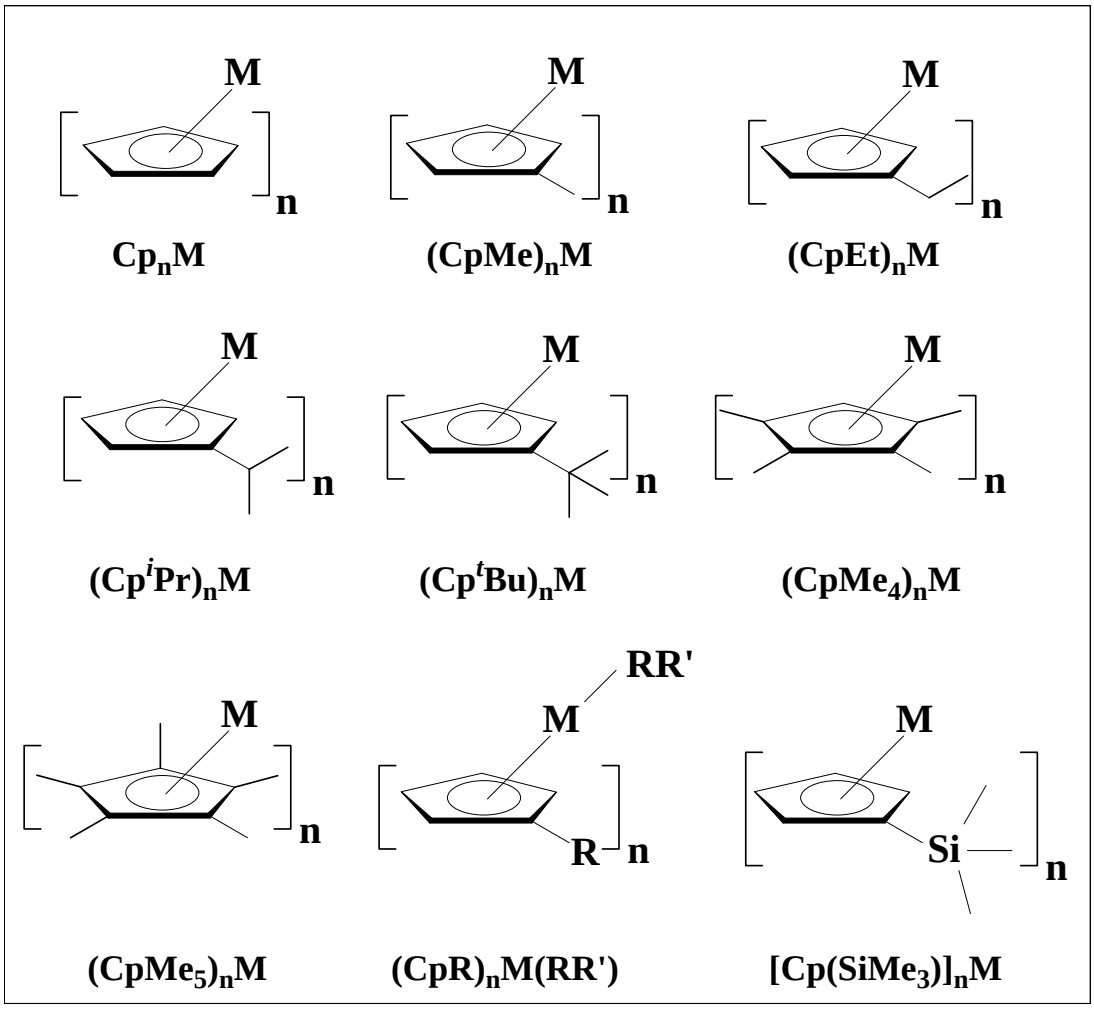

Figure 6. Examples of volatile cyclopentadienyl complexes for possible use as precursors in ALD. The R's represent alkyl groups such as Me or Et.

1.3.2 Oxygen sources

A long list of oxygen sources has been applied in the ALD of metal oxide thin films. They include H_2O, O_3, O_2, N_2O, H_2O_2, oxygen radicals, and metal alkoxides.[9,30] However, by far the most common oxygen source used is water. In the ALD of high-*k* oxides, one should consider also the oxidation power the oxygen source has towards the bare Si surface. This is crucial due to the fact that in order to achieve low EOT values, additional growth of low permittivity layers, *e.g.* SiO_x interfacial layer, should be minimized. When considering the oxidation power of commonly used oxygen sources, the following sequence can be written: Oxygen radicals > ozone > hydrogen peroxide > water. Unfortunately, the selection of oxygen precursor is in practice more complicated. A strong oxidizer, like ozone, can cause the formation of a fairly thick interfacial layer on H-terminated Si, *viz*.

approximately or usually more than 1 nm,[48-50,II,V] which may preclude ozone-processing as a long-term solution for gate dielectric fabrication. On the other hand, when compared to water, ozone can produce denser films with lower impurity levels and enhanced electrical properties.[50,51] Water-based processes rely on hydroxyl groups on the starting surface and high reactivity of the chemisorbed metal precursor towards the water pulse, otherwise the initial nucleation of the deposited films may be inhibited resulting in poor electrical properties of the deposited film.[52,53] In many cases, the metal precursor is not reactive enough towards the oxygen source and a stronger oxygen source must be used to deposit good quality film.[54] Until recently, comparative studies on the use of different oxygen sources in ALD of high-*k* oxides were seldom performed. One aim of this study was to evaluate the usability of ozone in ALD of high-*k* oxides and the results obtained will be discussed in detail in Chapter 3.

1.4 ALD of high-*k* dielectrics

As mentioned in Section 1.1, the leading candidates for alternative high-*k* dielectrics are the oxides, silicates, and silicate oxynitrides of Zr and Hf, as well as the oxides of the rare earths. As the selection of the precursor has an effect on the characteristics of the deposited film, this section emphasizes processes for the binary oxides, such as ZrO_2 and HfO_2, that are deposited with different types of precursors, and describes the current status of these materials. In this context, the Zr and Hf-based silicates are only briefly mentioned. Also, the less studied field of rare earth oxides by ALD will be discussed.

1.4.1 ZrO_2

The first ALD study on ZrO_2 published was the $ZrCl_4/H_2O$ process.[55] In that study, the growth temperature applied was 500°C, yielding a growth rate of 0.53 Å/cycle. Since then several groups have applied the same process in a wide temperature range of 180 to 600°C.[52,56-60] The optimized temperature found in most studies is 300°C, showing well-saturated growth with a growth rate of 0.5-1.0 Å/cycle, the exact value depending on the reactor set-up. Hydrogen and chlorine impurity levels at 300°C have been reported to be 0.6-0.8 and 1.5 at-%, respectively.[57] The chlorine level could be reduced by annealing at high (900-1050°C) temperatures.[61] However, annealing caused crystallization even in very thin layers.[62] The chlorine residues tend to accumulate at the interface region between the film and Si substrate.[63] Problems related to the $ZrCl_4/H_2O$ process include also the fact that

the metal precursor, being a fine solid, can generate particle contamination and the ALD reaction by-product is corrosive HCl.[64] In addition, the inhibited growth of zirconia on H-terminated Si, leading to an island-type growth,[52,65] remains as a challenge. A common solution to overcome this problem is to use thin thermal or chemical SiO_2 or nitrided SiO_2 as a starting layer. However, as lower *k* interfacial layer is introduced, to achieve sub-1.0 nm EOT values with low leakage becomes more difficult. For these obvious reasons alternative chemistries for the ALD of ZrO_2 has been the subject of much research. The reported ALD processes of ZrO_2 are listed in Table 2, including details of growth temperatures and impurities.

An option instead of using $ZrCl_4$ is to employ another Zr halide, namely ZrI_4.[66-69] Unfortunately especially for the high-*k* dielectric applications, ZrI_4 does not bring about any significant remedy to the problems mentioned above. The halide content remained at least at the same level as in the case of $ZrCl_4$ but presumably due to the weaker metal-halogen bond strength the annealing reduced the halide content more effectively.[70] On the other hand, it was observed that desorption of iodine caused problems for saturation of growth at 300°C.[67]

A distinct benefit of using Zr alkylamides, such as $Zr(NMe_2)_4$, $Zr(NEtMe)_4$, and $Zr(NEt_2)_4$ is that they are liquid at the evaporation temperature eliminating the particle contamination problem.[71] Furthermore, the alkylamides are reactive towards water and give impurity levels that are at least for C and N reasonably low, *e.g.* below 1 at-% for C.[71] However, higher C contents have been reported when oxygen or oxygen plasma was used as the oxygen source.[72-75] The problematic issue in the use of alkylamides is their thermal stability; *e.g.* for the $Zr(NMe_2)_4/H_2O$ process, the precursor decomposition limits the maximum growth temperature to 250°C. Furthermore, the growth temperature must be low if smooth films are desired.[76]

From the family of silylamide precursors, $ZrCl_2[N(SiMe_3)_2]_2$ has been applied together with H_2O to process zirconia yielding films with a few at-% of Si but low contents of C, H, and Cl.[77]

The limited thermal stability of Zr alkoxides represents a problem for their use in ALD. For instance, $Zr(O^tBu)_4$ has been employed with several oxygen sources[78-80] and even with

oxygen plasma,[72,81,82] but true ALD growth could not be achieved due to thermal decomposition of the metal precursor.[78,82] The decomposition behavior correlated with the impurity contents; 5-8 at-% of C has been reported for films deposited even at very low temperatures. Other approaches, like replacing two -O^{t}Bu ligands with dimethylaminoethoxide (dmae) ligands only slightly improved the thermal stability and self-limiting growth was not achieved.[83,84] Other solutions using the dmae-ligands were not successful, either.[83]

From the β-diketonate precursor group, $Zr(thd)_4$ has been used to grow ZrO_2 films.[85] Because of the low reactivity of the precursor, ozone was required as the oxygen source, but still a growth rate of only 0.24 Å/cycle was reported at deposition temperature of 375-400°C. ALD-type growth was confirmed and the contents of impurities were low, 0.2 and 0.3 at-% for C and H, respectively.

The use of cyclopentadienyl derivatives of Zr for ZrO_2 film growth was introduced quite recently.[85,I,II] Depositions from either Cp_2ZrCl_2 or Cp_2ZrMe_2 together with ozone showed an ALD-type growth with H and C residues less than 0.5 at-% and ZrO_2 growth rate of 0.55 Å/cycle within the ALD window regime, 300-350°C.[85] Cp_2ZrMe_2 could also be applied together with water[I] and this process, including reaction mechanism studies[III] and a comparison of structural and dielectric properties between the ozone- and water-processed films[II] is discussed in more detail in Section 3.1.

Table 2. Published ALD processes of ZrO_2 including growth temperatures and impurity characteristics.

Precursors		***T_{growth}***		***Impurities (at preferred T_{growth})***				
Metal precursor	**Oxygen source**	**Range, °C**	**Preferred, °C**	**C, at-%**	**H, at-%**	**Other, at-%**	**Analysis method**	**Ref.**
halides								
$ZrCl_4$	H_2O	180-600	300		1.5	Cl: 0.6-0.8	TOF-ERDA	55,57
	H_2O + H_2O_2	180-600	300		N.R.	N.R.		57,58
	O_2 *	500	500			N.R.		86
ZrI_4	H_2O + H_2O_2	230-500	275-325		3-8	I: 0.5-1.2	TOF-ERDA, XPS	66,68,69
amides								
$Zr(NEtMe)_4$	H_2O	< 250	< 250	< 1	N.R.	N: < 0.25	RBS	71
	O_2 [a]	110-250	200-250	1.6-3	N.R.	N: 0.3-3.5	AES, RBS	73
$Zr(NMe_2)_4$	H_2O	< 300	< 300	< 1	N.R.	N: < 0.25	RBS	71
$Zr(NEt_2)_4$	H_2O	< 350	< 350	< 1	N.R.	N: < 0.25	RBS	71
	O_2 [a]	250	250	1-3	N.R.	N.R.	AES	72
	O_2	250	250	3-5	N.R.	N.R.	AES	72
$ZrCl_2[N(SiMe_3)_2]_2$	H_2O	150-350	250	N.R.	N.R.	Si: 4	RBS, SIMS	77
alkoxides								
$Zr(O^tBu)_4$	O_2	250	250	6-8	N.R.	N.R.	AES	72
	O_2 [a]	250	250	3-5	N.R.	N.R.	AES	72,81
	H_2O	150-300	< 250	8	2	N.R.	TOF-ERDA	78
	N_2O	150-300	< 250	N.R.	N.R.	N.R.		79
$Zr(dmae)_4$	H_2O	190-340	190-340	5	30	N: < 4	TOF-ERDA	83
$Zr(O^tBu)_2(dmae)_2$	H_2O	190-340	190-340	1.7-3	8-13	N: 0.3-1.3	TOF-ERDA	83,84
$Zr(O^iPr)_2(dmae)_2$	H_2O	190-340	190-340	N.R.	N.R.	N: < 1	TOF-ERDA	83
β-diketonates								
$Zr(thd)_4$	O_3	275-500	375	0.2	0.3	F: < 0.1	TOF-ERDA	85
cyclopentadienyls								
Cp_2ZrMe_2	H_2O	200-500	350	< 0.1	< 0.1	N.R.	TOF-ERDA	I
	O_3	250-500	310-365	0.2	0.1	F: 0.1	TOF-ERDA	85
Cp_2ZrCl_2	O_3	200-500	300	0.5	0.5	Cl: < 0.07	TOF-ERDA	85

* atmospheric pressure, [a] plasma, N.R. = not reported

1.4.2 HfO_2

One of the most thoroughly studied ALD processes is the $HfCl_4/H_2O$ process, first introduced some 10 years ago.[87,88] Clearly, the interest in this process stems from the fact that in recent years HfO_2 has been identified as and continues to be considered one of the most promising high-*k* dielectrics.[3] Similarly as in the case of the $ZrCl_4/H_2O$ process, the obvious drawbacks of $HfCl_4/H_2O$ are well identified. The chlorine content, which is more pronounced near the HfO_2 film/silicon interfacial region,[89] has been reported to cause etching of the silicon substrate during post-deposition annealing, which contributes to void defect formation.[11] Additional problems include poor nucleation of HfO_2 when deposited directly on Si,[90] and formation of particles from the precursor in the gas phase. To overcome the problems related to the poor nucleation on HF-etched Si, the use of a thin chemically or thermally grown SiO_2, nitrided SiO_x, or interfacial layer of Al_2O_3 made by ALD has been suggested.[90] Nevertheless, additional interfacial layer increases the EOT value and in an ideal case a sharp interface between the Si and HfO_2 would be desirable. Despite the problems listed above, the $HfCl_4/H_2O$ process has many attractive features: the growth temperature range is wide, deposition temperatures ranging from 160 to 940°C have been reported,[91,92] the film quality and uniformity can be optimized over a large surface area,[90] carbon incorporation from the precursor into the films can be ignored, and good electrical properties, such as substantial leakage current reduction with respect to SiO_2, are well understood.[90] Due to the fact that $HfCl_4/H_2O$ growth process is so well optimized and established, finding a significantly better process is a challenging task.

The reported ALD processes for HfO_2 are listed in Table 3, where the alternative processes, as expected, are very similar to the previously described alternative ZrO_2 processes (Table 2). However, the influence of oxygen source has been studied in more detail in the case of HfO_2. Interestingly, replacing H_2O with O_3 in the $HfCl_4$-based process improves most of the dielectric properties, including fixed charge, interface trap densities, and the leakage current characteristics, as well as decreasing the Cl-content in the bulk of the film.[51] On the other hand, after rapid thermal annealing (RTA) at 750°C, higher oxygen content in the ozone-processed films resulted in thicker interfacial layer and thus increased CET. Commonly, the interfacial layer thickness in $HfCl_4/H_2O$ process at 300°C on HF-etched Si has been reported to be about 1.0-1.2 nm.[93]

A feasible route to Cl-free films is the use of HfI_4 instead of $HfCl_4$. The HfI_4/H_2O process yields slightly lower halide content in the films than the conventional $HfCl_4$ process when applied at 300 °C but the difference is not significant.[94] Using the iodide precursor with molecular oxygen eliminates hydrogen residues but the process requires rather high temperatures (500-750°C).[95,96]

The use of volatile, liquid hafnium alkylamides, especially $Hf(NEtMe)_4$, with water can provide excellent thickness uniformity and conformality[71] and excellent nucleation without significant interfacial layer formation on H-terminated Si,[97] but also yields films with considerable impurity content; *e.g.* 0.3-0.6 at-% of C and 2-3 at-% of H when $Hf(NEtMe)_4/H_2O$ ALD-process was applied at 250 °C.[98] The suitable ALD growth temperature range for the $Hf(NEtMe)_4/H_2O$ process is reported to be below 350°C[71] but slight decomposition of the precursor was probably affecting the growth rate already at temperatures around 300°C.[98] In another report, where the $Hf(NEtMe)_4/O_3$ process was applied, the maximum growth temperature suitable for good quality HfO_2 was 275°C.[99] The thickness of the interfacial layer between HfO_2 and H-terminated Si has been reported to be exceptionally low, ~0.5 nm for the $Hf(NEtMe)_4/H_2O$ process and problems in nucleation at early stages of the growth were not detected.[97] Interestingly, reaction with surface Si-H is initiated by the metal precursor, and not by the oxygen source.[100] It is worth noting that hydroxyl groups are incorporated into the HfO_2 film.[100] The interfacial SiO_2 then forms during annealing. Ozone as the oxygen source instead of water has gained considerable interest also in the case of $Hf(NEtMe)_4$ precursor to grow HfO_2[49,93,99,101,102] and especially together with a suitable Si-source, Hf-silicate.[22,102,103,104] However, in some studies the use of ozone did not significantly reduce impurities nor enhance electrical properties as compared to the use of water.[93,101] As compared with $Hf(NEtMe)_4$, higher impurity levels were detected in films obtained from $Hf(NMe_2)_4$ and water[105] or ozone.[115] Signs of thermal decomposition of the $Hf(NMe_2)_4$ precursor were detected already at 250°C.[105] In addition, the surface roughness increased rapidly at temperatures around 250°C.[76] When using the $Hf(NMe_2)_4/H_2O$ process, it was recently proposed that during the early stages of HfO_2 growth on H-terminated silicon, a SiN_x interfacial layer is formed instead of SiO_2, thus yielding a very promising CET of 1.8 nm with low leakage current density.[107] However, in another study a relatively thick 1.5-2.0 nm interfacial silicon oxide layer was observed between Si and amorphous HfO_2.[105] Using ozone instead of water at a relatively high growth temperature of 300°C reduced the impurity contents and the films

showed a more amorphous structure leading to better leakage current characteristics.[108,109] A third Hf-alkylamide precursor, $Hf(NEt_2)_4$, has been used occasionally, together with either water,[71,110] oxygen,[111] or oxygen plasma[111-114] as the oxygen source. Especially in the case of oxygen plasma, the growth of interfacial Hf-silicate layer can be significant.[111,112]

As in the alternative ZrO_2 processes, the alkoxide-based processes of HfO_2 generally suffer from poor thermal stability of the Hf-precursor.[81,82,115-119] Due to the decomposition of the precursor, carbon and hydrogen impurities remain high, *e.g.* the ALD process employing hafnium tetrakis(1-methoxy-2-methyl-2-propanolate), $Hf(mmp)_4$ with H_2O at 360 °C resulted in as-deposited films with 12 and 6 at-% of C and H, respectively.[118]

Anhydrous volatile $Hf(NO_3)_4$ has also recently been applied as an ALD precursor for the deposition of oxygen-rich hafnium oxide films.[33,120] A promising CET value of 2.1 for a 5.7 nm film deposited directly on H-terminated Si was reported, but the precursor decomposition limits its use to only very low temperatures of 180 °C or lower.[33]

Another precursor family exhibiting both high reactivity and volatility are the cyclopentadienyl compounds of hafnium, which have recently been introduced in ALD for high quality HfO_2 film growth.[IV,V] Section 3.2 describes the growth characteristics and HfO_2 film properties obtained with the Cp-based hafnium processes. For comparison, compositional data of the films deposited with the Cp-precursors are also included in the Table 3.

Table 3. Published ALD processes for HfO_2 with reported impurities.

Precursors		***T_{growth}***		***Impurities (at preferred T_{growth})***				
Metal precursor	**Oxygen source**	**Range, °C**	**Preferred, °C**	**C, at-%**	**H, at-%**	**Other, at-%**	**Analysis method**	**Ref.**
halides								
$HfCl_4$	H_2O	160-940	300		0.5-1.5	Cl: 0.4	TOF-ERDA	51,88,90-92,94
	O_3	300	300		N.R.	N.R.		51
	O_2*	250-650	550-650			Cl: 0.1	XPS, SIMS	121
	$Hf(NO_3)_4$	150-190	150-190		N.R.	N.R.		122
HfI_4	H_2O	225-500	300		1.5	I: 0.4	TOF-ERDA	94
	O_2	400-755	570-755		< 0.1	I : < 0.1	TOF-ERDA	95,96
amides								
$Hf(NEtMe)_4$	H_2O	100-450	250	0.3-0.6	2-3	N: < 0.2	TOF-ERDA	71,98
	O_3	100-400	250-300	1.5	N.R.	N.R.	AES	115
$Hf(NMe_2)_4$	H_2O	100-500	250	1.5	6	N: < 0.7	TOF-ERDA	71,105,123
	O_3	160-420	200-300	4.5	N.R.	N.R.	AES	115
$Hf(NEt_2)_4$	H_2O	100-500	<450	< 1	N.R.	N: < 0.25	RBS	71
	O_2	250	250	5	N.R.	N.R.	AES	111
	O_2[a]	250	250	2.5	N.R.	N.R.	AES	111
$HfCl_2[N(SiMe_3)_2]_2$	H_2O	150-250	200	< 1	< 1	N: < 1	AES	124
alkoxides								
$Hf(O^tBu)_4$	O_2	350-480	350-480	N.R.	N.R.	N.R.		116
	O_3	300-450	300	6	N.R.	N.R.	AES	115,125,126
	O_2[a]	200-250	200	N.R.	N.R.	N.R.		82
$Hf(O^tBu)_2(mmp)_2$	H_2O	275-400	360	2.7	11	N.R.	TOF-ERDA	117
$Hf(mmp)_4$	H_2O	225-450	225-360	0.8-6	12	N.R.	TOF-ERDA, AES	118,127
$Hf(ONEt_2)_4$	H_2O	250-350	300	6	11	N: < 1	TOF-ERDA	119
cyclopentadienyls								
Cp_2HfMe_2	H_2O	300-500	350	0.4	0.2	N.R.	TOF-ERDA	IV,V
	O_3	275-450	350	< 0.1	< 0.1	N.R.	TOF-ERDA	V
Cp_2HfCl_2	H_2O	350	350	1.2	0.5	Cl: 0.4	TOF-ERDA	V
	O_3	350	350	< 0.3	< 0.3	Cl: < 0.1	TOF-ERDA	V
Other								
$Hf(NO_3)_4$	H_2O	160-190	180		N.R.	N: 1.2	XPS	33,120

* atmospheric pressure, [a] plasma, N.R. = not reported

1.4.3 Rare earth oxides

The ALD of rare earth oxides generally suffers from the lack of suitable precursors. The first ALD processes for RE oxides were reported in the early 1990s, introducing β-diketonate precursors together with a strong oxygen source, ozone, to grow Y_2O_3[128] and CeO_2[129] films. Since then new classes of precursors have been introduced which can be conveniently divided into three categories according to the ligand donor atom; namely oxygen-, carbon-, and nitrogen-coordinated precursors. Here the reported RE oxide processes are considered only briefly, a more detailed survey has been recently reported by Päiväsaari *et al.*[130] For more specialized reviews emphasizing gate dielectrics in microelectronics, see also Leskelä *et al*.[131,132]

Typically the existing RE oxide ALD processes have been based on the oxygen-coordinated β-diketonate precursors, such as the thd-complexes (thd=2,2,6,6-tetramethyl-3,5-heptanedione) from which almost all RE binary oxides, except the oxides of Pr, Pm and Tb, have been grown.[24,48,128,129,133-138,VIII] As thd-compounds are not reactive enough towards water, ozone was required as oxygen source. Typically the deposition temperature for an optimized RE oxide ALD process has been 300°C.[24] Interestingly, it was reported that growth rate at 300°C increased linearly as a function of the ionic radius of the lanthanides, suggesting the same growth mechanism regardless of the metal.[24] The $RE(thd)_x/O_3$ processes generally produce oxygen deficient films with C and H impurities around 1-5 and 1-2 at-%, respectively.[24] Deviations in the carbon content are caused by the difference in basicity of the RE oxides, resulting in large content of carbonate-type impurities for the larger ions, *e.g.* La_2O_3 contained up to 10-12 at-% of carbon,[134] but Sc_2O_3 only less than 0.1 at-%.[133] The growth rates in thd-based RE oxide processes are generally low, caused by the considerable steric hindrance and low reactivity. To increase the growth rates radical enhanced ALD has also been applied.[139,140] Unfortunately, carbon content was thereby further increased, up to 26 at-% in Er_2O_3 films.[139] Oxygen-coordinated precursors other than those based on the thd ligand have been only occasionally applied, *e.g*. ALD of Gd_2O_3 and PrO_x from $Gd(mmp)_3$ and $Pr(mmp)_3$ with water as oxygen source was recently reported.[127] Unfortunately, self-limiting growth was not achieved due to precursor decomposition.

Among the nitrogen-coordinated precursors, silylamides and amidinates have especially gained recent interest as potential ALD precursors. Silylamide compounds of La, Gd and Pr may provide a feasible route to grow high-*k* La_2O_3,[123,141-143] Gd_2O_3,[35,36] and PrO_x[144] films. At least in the case of $Ln[N(SiMe_3)_2]_3/H_2O$ (Ln=Gd,Pr) processes, self-limiting growth could not be observed due to the precursor decomposition, resulting also in considerable impurity contents.[35,36,144] The $La[N(SiMe_3)_2]_3/H_2O$ process, however, was reported to be saturative at 200-275°C, but about 10 at-% of Si was determined to be present in the deposited films.[142] In another recent study, the thermal decomposition of $La[N(SiMe_3)_2]_3$ could not be excluded as a possible factor affecting the growth behavior.[145]

Another interesting approach to ALD of RE oxide films is based on the use of amidinate complexes of the composition $RE[RamdR]_x$ (R=alkyl group, amd=$NC(CH_3)N$). The $[^{i}Pramd^{i}Pr]_3$ complexes of Y, Sc, La have been applied by Gordon and coworkers using water to form Y_2O_3,[146] Sc_2O_3,[147] and La_2O_3[41] films. In a more detailed report, the Y_2O_3 process was found to be promising, as the conformality and dielectric properties were good.[146] Thermal stability may call for attention, as $Y[^{i}Pramd^{i}Pr]_3$ decomposition became evident at temperatures exceeding 280°C.[146] In another study, Er_2O_3 films were grown using $Er[^{t}Buamd^{t}Bu]_3$ and ozone.[42] Water was not reactive enough as an oxygen source, because of higher steric hindrance caused by the *tert*-butyl groups compared to the *iso*-propyl groups. On the other hand, *tert*-butyl groups should be more protective towards decomposition of the complex and thus the thermal stability should be better.[148] However, self-limiting growth of Er_2O_3 could not be achieved due to the probable partial decomposition of $Er[^{t}Buamd^{t}Bu]_3$, considering that upon increasing the precursor pulse length the growth rate also increased.[42] One possible reason for this behavior was suggested: In the $Y[^{i}Pramd^{i}Pr]_3/H_2O$ process, the adsorption of some water during the water pulse followed by desorption of water could result in a water-rich ambient above the film. This would lead to a CVD-type growth if purging times are not very long.[146] Therefore, purge time for water used in the $Y[^{i}Pramd^{i}Pr]_3/H_2O$ study was 60 s.[146] However, a 5-fold increase in purge times in the $Er[^{t}Buamd^{t}Bu]_3/O_3$ process did not have any effect.[42] On the other hand, in ozone processes the growth mechanism is different than in water processes. Generally, very long purge times would make a process practically unfit for applications, but at the same time, dielectric properties could be enhanced due to the annealing effect achieved during the deposition.

Interest in true organometallic compounds for application in ALD of RE oxides is currently focused on the cyclopentadienyl compounds. As suitable metal alkyls do not exist for rare earths, volatile and reactive Cp-compounds have been applied in several RE oxide growth studies.[133,VII-IX,149] More detailed discussion on the applicability of RE Cp-compounds as well as an introduction to various $REScO_3$ processes are presented in Section 3.3.

2. EXPERIMENTAL

This chapter briefly presents the methods used for film growth studies and for the characterization of the deposited films, as well as explains how the *in situ* reaction mechanism studies were performed. More detailed descriptions including, when relevant, precursor synthesis, properties and pulsing sequences can be found in the original publications I-IX. For the processes not reported earlier, the growth characteristics are described in chapter 2.1.

2.1 Precursors and film growth

High-*k* oxide films were deposited in a commercial flow-type hot-wall ALD reactor (ASM Microchemistry F-120). As precursors, thd- or cyclopentadienyl-type compounds were applied together with the oxygen source (O_3 or H_2O). Because of their air and moisture sensitivity, the cyclopentadienyl precursors were handled in an Ar glove box and inertly inserted into the reactor. The metal precursors were evaporated from an open glass crucible inside the reactor. Ozone was generated from O_2 (99.999%) in an ozone generator (Fischer model 502). The ozone concentration as determined by iodometric titration was about 4 %.[133] Water was evaporated from a container kept at 25°C. Precursors used in this study are listed in Table 4, where also their origin and the evaporation temperatures are shown. Depositions were carried out at 2-3 mbar pressure. Nitrogen (99.999%) was used as a carrier and purging gas except in the reaction mechanism studies, where Ar (99.999%) was used. As substrates, p- or n-type Si(100) (Okmetic, Finland) and sodalime glass were used. The substrate area was 10 x 5 cm^2. HF-etching of the Si-substrate immediately prior to the deposition was applied in selected experiments in order to remove the native SiO_2. The standard pulsing sequence for the binary water-based processes where as follows: 1.0-1.5 s metal precursor pulse, 1.5 s purge, 1.5 water pulse, 1.5 s purge. When ozone was applied, the oxygen source pulse time and the following purge time were both 2.0 s. The metal precursor pulse time was varied between 1.0 and 3.0 s in order to study the saturation characteristics. For the novel ternary processes, $GdScO_3$ and $ErScO_3$, the pulsing sequence was similar as that used for $YScO_3$.[IX]

Table 4. The sublimation/evaporation onset temperatures and the source of the precursors applied for ALD studies of oxide materials. The precursors are solid at sublimation/evaporation temperature, unless indicated otherwise.

Film material	Precursor	Sublimation/ Evaporation T at 2-3 mbar, °C		Precursor source
ZrO_2	Cp_2ZrMe_2	70		[150]
HfO_2	Cp_2HfMe_2	70		[150]
	Cp_2HfCl_2	135-140		Strem Chemicals Inc.
Y_2O_3, $YScO_3$	$Y(thd)_3$	125		[151]
	$(CpMe)_3Y$	110	(partly liq.)	Russian Academy of Sciences*
	Cp_3Y	150		Strem Chemicals Inc.
	$Sc(thd)_3$	115		[151]
	Cp_3Sc	150-155		Russian Academy of Sciences*
La_2O_3	Cp_3La	250		Strem Chemicals Inc.
	$(CpMe)_3La$	165-170		Russian Academy of Sciences*
	$(CpMe_4)_3La$	175		Sigma-Aldrich, Inc.
	$(Cp^iPr)_3La$	140	(liquid)	Strem Chemicals Inc.
PrO_x	$(CpMe_4)_3Pr$	175	(liquid)	Sigma-Aldrich, Inc.
	$(Cp^iPr)_3Pr$	140-145	(liquid)	Sigma-Aldrich, Inc.
Gd_2O_3, $GdScO_3$	$Gd(thd)_3$	140		[151]
	$(CpMe)_3Gd$	110		Russian Academy of Sciences*
	$(CpMe_4)_3Gd$	175-178		Sigma-Aldrich, Inc.
Er_2O_3, $ErScO_3$	$(CpMe)_3Er$	115		Russian Academy of Sciences*

* Institute of Organometallic Chemistry, Russian Academy of Sciences, Nizhny Novgorod, Russia

2.2 Film characterization

The oxide thin films were analyzed by various techniques for their composition, thickness, morphology, structure, and electrical properties. Table 5 lists the techniques used in this thesis and also summarizes the information obtained.

The thickness of the deposited films was determined by measuring the optical reflectance spectra (Hitachi U-2000 double beam spectrophotometer) in the wavelength range of 190 to 1100 nm and fitting a theoretical spectrum to the measured spectrum.[152] In addition, the

thickness, roughness, density and crystal structure of selected ultrathin films were evaluated by X-ray reflectometry (XRR) and by grazing incidence X-ray diffraction (GI-XRD) using a Bruker D8 Advance X-ray diffractometer. Crystallite orientations and crystallinity of the deposited films were determined by X-ray diffraction with Cu Kα radiation in a Philips MPD 1880 diffractometer. High-resolution transmission electron microscopy (HR-TEM) was also applied in order to examine the cross-section of an ultrathin sample as well as the interfacial layers between selected deposited films and the silicon substrate. The high-resolution images were obtained with a field emission gun TECHNAI F30 ST or Hitachi: H9000NAR, both operated at 300 kV. To investigate the composition of the interfacial layer, X-ray photoelectron spectroscopy (XPS) was applied. The measurements were carried out in an AXIS 165 spectrometer (Kratos Analytical) using monochromated Al K_α irradiation at 100 W. Surface morphology was studied with a Nanoscope III atomic force microscope (AFM), by Digital Instruments, operated in tapping mode. Roughness values were calculated as root mean square (rms) values.

Film compositions were measured by time-of-flight elastic recoil detection analysis (TOF-ERDA)[153] at the Accelerator Laboratory of the University of Helsinki, Finland and at IMEC (Interuniversity Microelectronics Center), Leuven, Belgium. For these TOF-ERDA studies, 53 MeV $^{127}I^{10+}$ or 16 MeV $^{63}Cu^{7+}$ ion beams were used. Metal to metal ratio in scandate films were also analysed by XRF (Philips PW 1480) using Rh excitation. In order to obtain more information on residual carbon and hydrogen impurities, the films were also analyzed by Fourier-transform infrared (FTIR) spectroscopy. The FTIR single-beam transmission spectra were collected from the samples deposited on Si with Nicolet Magna-IR 750 spectrometer.

For electrical characterizations, aluminum gate electrodes for ohmic contact were formed by e-beam evaporation onto the HF-etched backside of the substrate as well as through a shadow mask onto the film surface. The resulting capacitor structures were then measured with a HP 4284A precision inductance-capacitance-resistance-meter and Keithley 2400 source meter to obtain capacitance-voltage (*C*-*V*) and leakage current density-voltage (*I*-*V*) characteristics, respectively. The effective permittivity values were calculated from the accumulation capacitance using equation (1) and thus the CET values and the permittivity for the high-*k* layer only from equations (2) and (3).

Table 5. Film characterization techniques used.

Technique	Information obtained	Publication
AFM	Surface morphology	I, II, IV-IX
Electrical measurements		
C-V	Dielectric properties	I, II, IV-IX
I-V	Leakage current	I, II, IV-IX
FTIR	Carbonate and hydroxide impurities	I, VI, VIII, IX
GI-XRD	Crystallinity	I, II
HR-TEM	Interfacial layer, microstructure	I, II, V
QMS	Reaction mechanism	III
Spectrophotometer	Thickness	I, IV-IX
TOF-ERDA	Impurities, stoichiometry	I, IV-IX
XPS	Interfacial layer composition	II
XRD	Crystallinity, crystalline phases	I, II, IV-IX
XRF	Stoichiometry	IX
XRR	Thickness, density, interface	I, II, IV, V, IX

2.3 Reaction mechanism studies

Experiments to resolve the reaction mechanism for the ZrO_2 process from Cp_2ZrMe_2 precursor were carried out in a commercial, but specially modified, flow-type F-120 ALD reactor. The reaction chamber was loaded with glass substrates in order to form narrow gas flow channels between them with large substrate area. To maximize the amount of reaction by-products, the total area of glass substrates was about 3500 cm^2. The gas phase species were measured with a Hiden HAL/3F 501 RC quadrupole mass spectrometer (QMS) using an electron multiplier detector, mass range of 1 - 510 amu and ionization energy of 70 eV. The sampling and the pressure reduction from about 2 mbar to below 10^{-6} mbar were accomplished through a 200 μm opening. Instead of H_2O as the oxygen source, D_2O was used in order to better distinguish the reaction by-products from the species formed in the ionizator.

Weak background signals arise also even when no exchange reactions should take place, *i.e*. when subsequent pulses of only one precursor are given. This background signal, suggested to be caused by a condensation effect of the metal precursor, pressure change effects, insufficient mass resolution of the QMS or possible rearrangement reactions during ionization,[154] is subtracted from the signals obtained during the actual ALD process. The thermal stability of the Cp_2ZrMe_2 precursor was studied also with the QMS by pulsing only the precursor and monitoring the ligand decomposition products detected as a function of deposition temperature.

3. RESULTS AND DISCUSSION

This chapter summarizes the main results of ZrO_2, HfO_2, and rare earth oxide film growth and characterization. Details for the published processes can be found in the corresponding publications.[I-IX]

3.1 ZrO_2 from cyclopentadienyl precursor

ALD-type self-limiting growth was achieved by applying Cp_2ZrMe_2 and H_2O as precursors.[I] The growth rate increased as a function of deposition temperature and a distinct ALD window was not observed. At the optimized deposition temperature of 350°C the growth rate was 0.43 Å/cycle resulting in polycrystalline films. The monoclinic phase was the dominant one, but minor intensity reflections belonging to the orthorhombic phase were also observed. At growth temperatures lower than 300°C the growth rate remained low, indicative of insufficient thermal energy to promote fast surface reactions. At temperatures exceeding 400°C, poor uniformity of the films was observed due to precursor decomposition. Interestingly, the roughness of 100-130 nm thick films decreased when the deposition temperature was increased from 375 to 400°C. At 350°C the impurity contents for the stoichiometric ZrO_2 films were below the detection limit (~0.1 at-%) of TOF-ERDA for both C and H. The impurity levels were lower than most of the other known ZrO_2 ALD processes (see Table 2). It is worth noting, that the present Cp_2ZrMe_2/H_2O process results in films with good thickness uniformity over large substrate areas, as demonstrated in scale-up tests on 200 mm Si wafer (Figure 7).

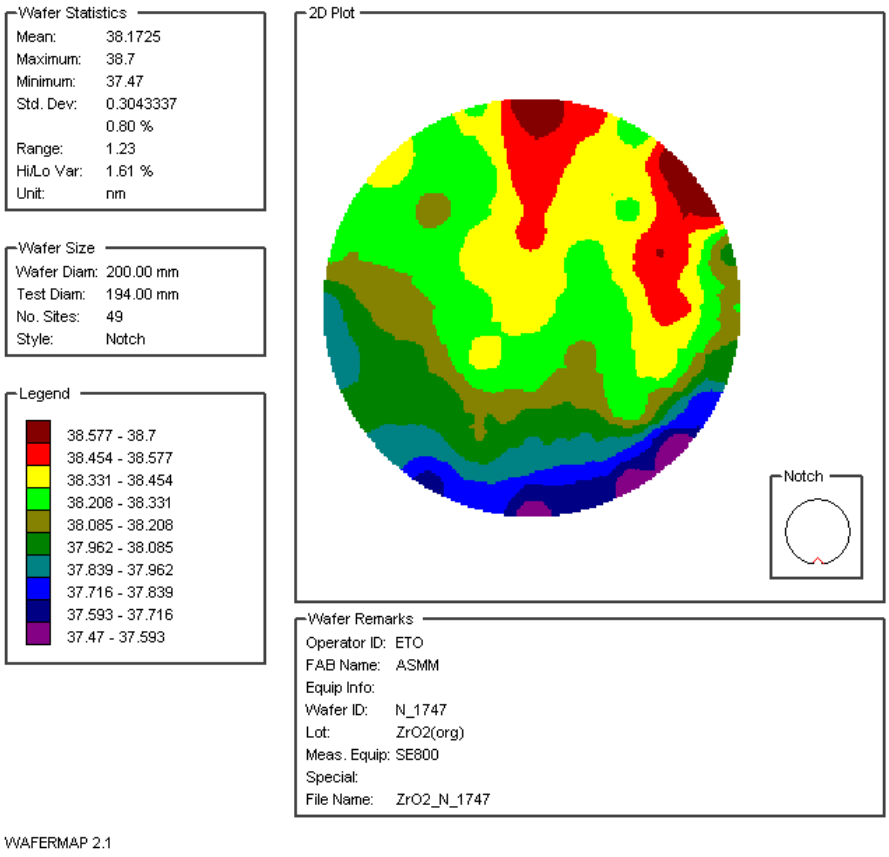

Figure 7. The variation of thickness in ZrO_2 thin film deposited by ALD at 300°C by the Cp_2ZrMe_2/H_2O process on 200 mm Si-wafer. The mean thickness of the ZrO_2 layer is 38.2 nm and the standard deviation 0.80 %. (Courtesy of ASM Microchemistry Ltd.)

When ozone was applied as the oxygen source, the growth rate of ZrO_2 films increased to 0.55 Å/cycle.[II] Ozone, being a more aggressive oxidant than water, had a strong effect on the growth behavior, structure, and electrical properties, especially when ZrO_2 was deposited on H-terminated (HF-etched) Si. When water was used as the oxygen source, a strong inhibition of film growth at the early stages of the deposition process was clearly detected. As seen in Figure 8, ozone oxidizes the bare Si surface, creating an interfacial SiO_x layer, which is a suitable surface for the film growth to proceed. Water, however, is not able to form OH-saturated surface for the metal precursor to react with and thus retarded nucleation leads to island-like growth and reduced density (Figure 8).[II]

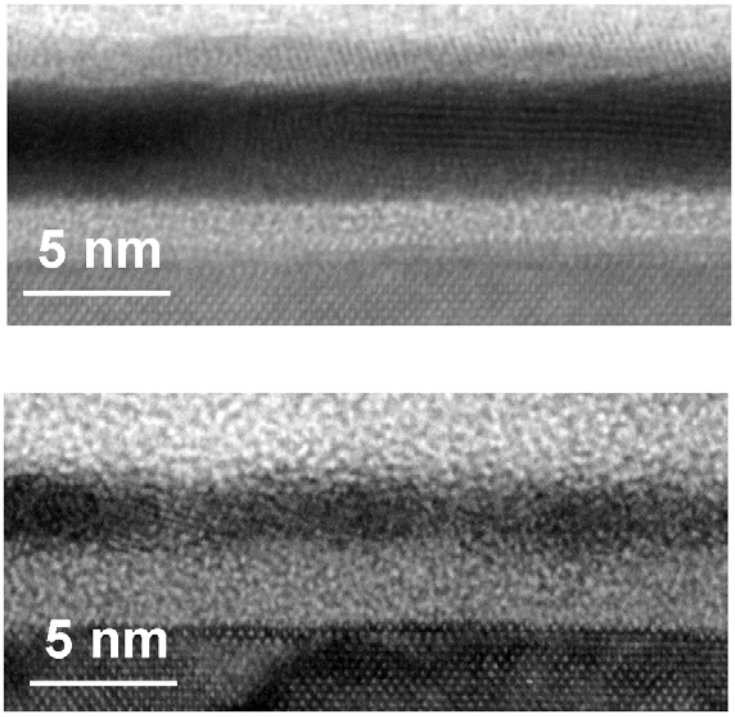

Figure 8. HR-TEM images of the ZrO_2 films deposited onto HF-etched Si(100) by the (top) Cp_2ZrMe_2/O_3 (ZrO_2 thickness 3.8 nm, IL thickness 1.9 nm) and (bottom) Cp_2ZrMe_2/H_2O (ZrO_2 thickness: 2.1 nm, IL thickness 2.9 nm) process.[II]

Inhibition of growth has also been detected with the other ZrO_2 processes where water is used as the oxygen source.[52] The interfacial layer formed in the water-processed films, according to the electrical and XPS measurements, is suggested to be a mixture of SiO_x and ZrO_2 rather than Zr-silicate.[II] Similar intermixing in the interfacial layer has been observed previously, when $ZrCl_4/H_2O$ process was applied on chemical SiO_2.[56]

The oxygen source and substrate pretreatment had a distinct effect on the electrical properties of the Al/ZrO_2/native SiO_2 or HF-etched/n-Si(100) capacitor structures. The hysteresis width was extremely low for both H_2O- and O_3-processed HfO_2 films on HF-etched Si (Figure 9). With both processes, the as-deposited films showed flatband voltage (V_{FB}) shift; in O_3-processed films towards negative bias and in H_2O-processed films towards positive bias. Forming gas annealed (5 % H_2, 400°C, 30 min) O_3-processed samples exhibited almost the ideal value of V_{FB}. Annealing also reduced the interface state density values. The permittivity of an 8.8 nm O_3-processed film was approximately 20.

The $Cp_2Zr(CH_3)_2/H_2O$ process on native oxide-free Si resulted in structures with high but not completely saturative accumulation capacitance (Figure 9). For example, the as-deposited insulator structure with a 5.9 nm ZrO_2 film had a CET value of 2.0 nm and an effective permittivity of 11.4. As mentioned previously, the interfacial layer is thought to be a mixture of ZrO_2 and SiO_2 having a greater permittivity than that of SiO_2. However, an inhomogeneous microstructure arising from the inhibited growth on the H-terminated surface resulted in higher leakage current for the water-processed films (Figure 9b).

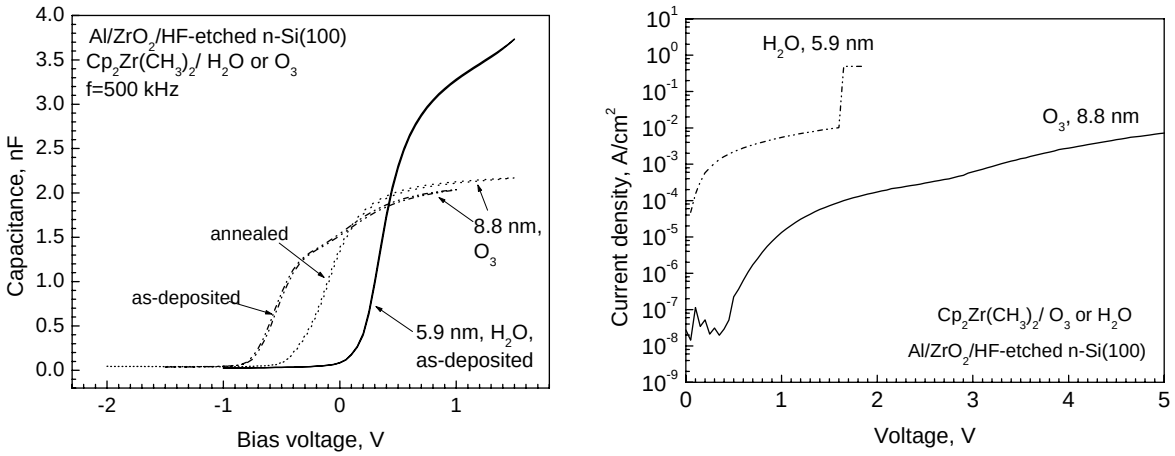

Figure 9. The *C-V* (a) and *I-V* (b) curves of Al/ZrO_2/HF-etched Si structures. Labels indicate the oxygen precursor used and the ZrO_2 layer thickness.[II] For Al/insulator/n-Si(100) structure, the V_{FB} should be around -0.2 V.[155]

Figure 10 shows the capacitance equivalent oxide thickness as a function of the ZrO_2 film physical thickness for the different precursor and surface pre-treatment combinations. The CET values were comparable for films deposited with water or ozone onto native oxide covered Si as well as for those deposited with ozone onto HF-etched Si. The CET of the interfacial layer is obtained from the plot of CET *vs.* ZrO_2 thickness as the y-intercept and assuming the IL to have constant permittivity of 3.9, the intercept with the y-axis equals the physical thickness of the IL. The determined IL value of 2 nm is supported well by the HR-TEM results (Figure 8 top). From the slope, permittivity values of about 20 can be calculated for the ZrO_2 layer. However, for the H_2O process on HF-etched Si, low CET values were obtained and the intercept can occur below 2 nm. The HR-TEM results showed considerably thicker IL (Figure 8 bottom). This indicates again that the interfacial oxide has a greater permittivity than SiO_2 due to the intermixing of SiO_2 and ZrO_2 as discussed above.[II]

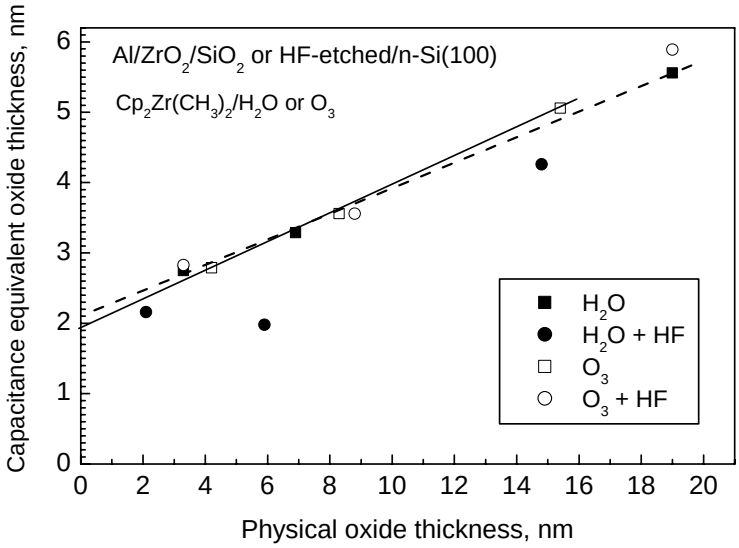

Figure 10. Calculated capacitance equivalent oxide thickness as function of the physical oxide thickness measured by XRR. Inset labels denote the oxygen precursor. HF indicates a surface pre-treatment with HF-etching. Otherwise, the films were grown onto Si substrates covered by native oxide.[II]

3.1.1 Reaction mechanism studies

The *in situ* QMS data of the Cp_2ZrMe_2/D_2O process suggest that the reaction byproducts observed were CpD and MeD.[III] As well established for the ALD growth of oxide thin films, the number of –OH groups left on the surface after the water pulse is an important factor for controlled growth.[9] Thus, it can be suggested that ZrO_2 grows in the present Cp_2ZrMe_2/D_2O process via exchange reactions with OD-terminated surface as the starting surface:

$$(x+y)\text{-OD (s)} + Cp_2ZrMe_2\ (g) \rightarrow (\text{-O-})(x+y)ZrCp_{2-x}Me_{2-y}\ (s) + y\ MeD\ (g) + x\ CpD\ (g) \quad (4)$$

$$(\text{-O-})_{(x+y)}\ ZrCp_{2-x}Me_{2-y}\ (s) + 2\ D_2O\ (g) \rightarrow (\text{-O-})_2Zr(OD)_{x+y}(s) + (2-x)\ CpD\ (g) + (2-y)\ MeD\ (g) \quad (5)$$

In the present study, nearly all (~90 %) MeD was released during the Cp_2ZrMe_2 pulse in the exchange reactions with the surface OD groups. In addition, about 40 % of the Cp ligands were released during the metal precursor pulse. The following D_2O pulse converted the surface back to an OD-saturated one by releasing the remaining CpD and MeD. After this cycle the OD-saturated surface is regained and ready for the next deposition cycle. The proposed mechanism at 350°C is presented in Figure 11.[III]

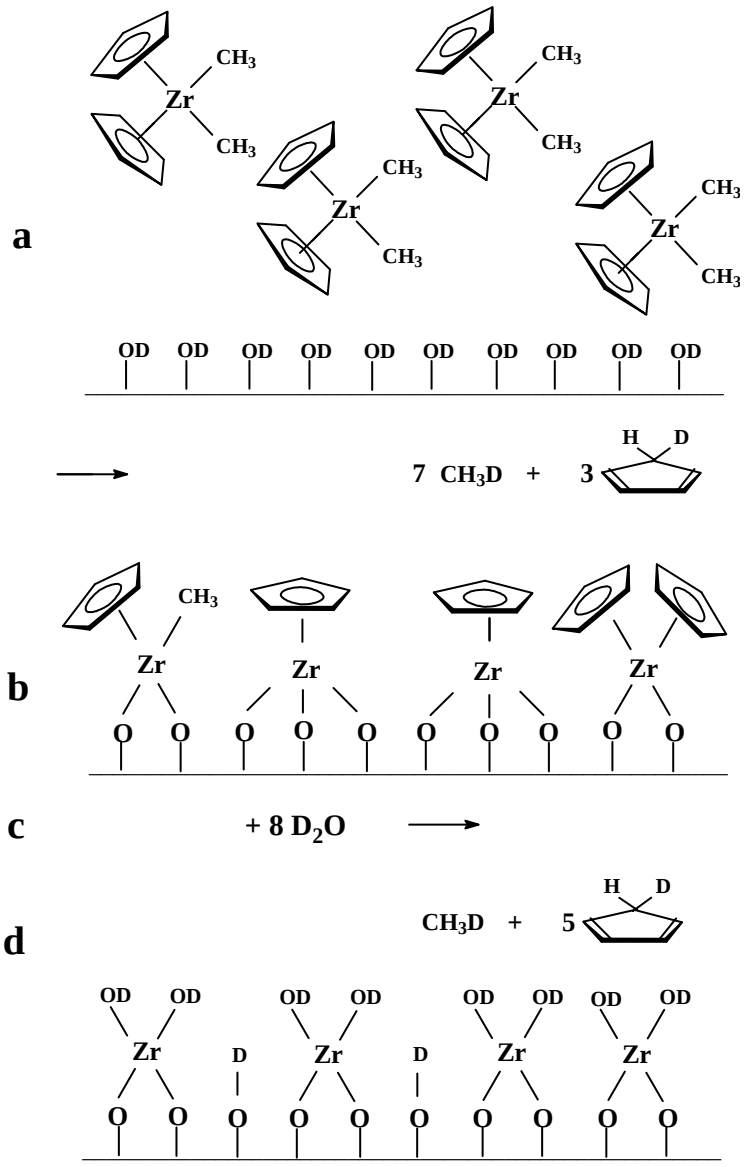

Figure 11. Proposed reaction mechanism of Cp_2ZrMe_2/D_2O ALD process at 350°C.[III]

The reaction mechanism is only weakly dependent on the deposition temperature until the thermal decomposition of $Cp_2Zr(CH_3)_2$ started which then played a role in the mechanism at deposition temperatures exceeding 400°C. First signs of partial decomposition of the Cp_2ZrMe_2 could be observed at 375°C.

3.2 HfO_2 from cyclopentadienyl precursors

By applying cyclopentadienyl-type precursors for HfO_2, similar growth characteristics were observed as in the ZrO_2 film deposition from the Cp_2ZrMe_2 precursor. The growth rate of the polycrystalline HfO_2 films by the Cp_2HfMe_2/H_2O process was 0.42 Å/cycle at optimized growth temperature of 350°C.[IV] The growth rate increased to 0.54 Å/cycle when O_3 was applied as the oxygen source.[V] These values can be compared to those obtained for ZrO_2: 0.43 and 0.55 Å/cycle.[I,II] Saturation of the growth rate was confirmed at 350°C. At that temperature alkylamide- and alkoxide-based alternative HfO_2 processes suffer from precursor decomposition (Table 3). In the present case, promoted by the stronger oxidation power of O_3, films could be deposited with reasonable growth rates at 300°C while with water the growth rate was low, or 0.1 Å/cycle. Above 400°C, the precursor decomposition degraded the film uniformity over the substrate area. At 350°C, films grown by the Cl-containing Cp-precursor, Cp_2HfCl_2 exhibited comparable growth rates to those provided by Cp_2HfMe_2.[V] Generally, the growth rate of HfO_2 in the current Cp-based processes is somewhat lower than that of 0.7-1.0 Å/cycle obtained by the alkylamide-based processes.[98,105]

According to the TOF-ERDA studies, films deposited from Cp_2HfMe_2 were stoichiometric with low levels of C and H as impurities (Figure 12).[IV,V] However, due to the different growth mechanism, and ozone being more aggressive oxidizer than water, the surface reactions seem to be more complete with ozone resulting in lower impurity contents: *viz*. below 0.1 at-% for C and H at growth temperatures of 350 and 400°C. In the films deposited with the Cp_2HfCl_2, some chlorine was detected. As the Cp_2HfCl_2 precursor caused Cl-contamination into the films, a drawback also recognized in the well-studied $HfCl_4$-based ALD-processes,[89,94] further studies with the Cp_2HfCl_2 precursor were discontinued. It can be concluded here that the current approach using Cp-based precursors seems to result in films with higher purity than the other precursor combinations studied (Table 3).

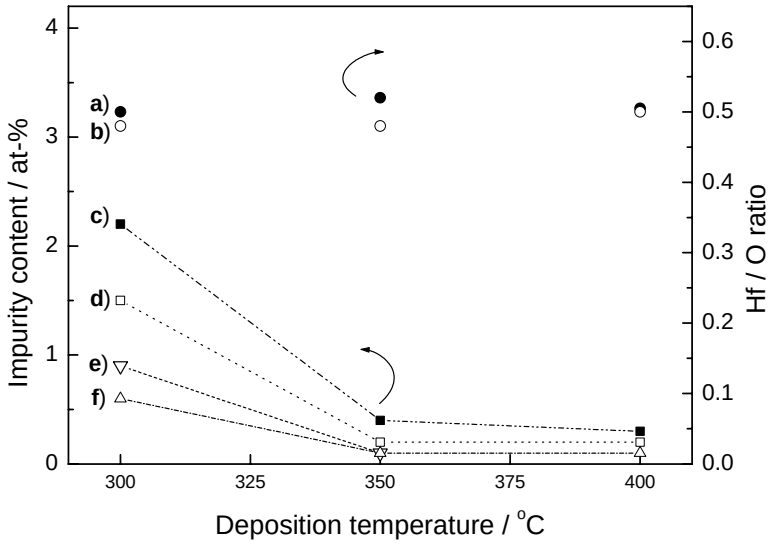

Figure 12. Observed Hf/O ratio at different deposition temperatures in the HfO_2 films deposited from Cp_2HfMe_2 and water (a) or ozone (b). In addition, the hydrogen contents using water (c) or ozone (e) as well as the carbon content using water (d) or ozone (f) are plotted at different deposition temperatures.[V]

An inhibition of growth at the early stages of the deposition on H-terminated Si similar to that detected for the water-based processes using $HfCl_4$[90] or Cp_2ZrMe_2,[II] was also observed in the current Cp_2HfMe_2/H_2O process.[V] Si-H bonds are not effectively replaced by water to create an OH-terminated surface suitable for oxide film growth, a behavior which lead to island nucleation, and thus, decreased film density and increased surface roughness (Figure 13).[V] Such a retarded growth was not observed, however, when ozone was used as an oxygen source, for which a linear relation between thickness and number of deposition cycles applied was observed. In addition, film roughness remained very low (Figure 13) and the density was close to the bulk value (9-10 g/cm^3). The interfacial layer thickness between the H-terminated Si and HfO_2 layer was about 0.5 nm and 1 nm for the H_2O- and O_3-based processes, respectively. It should be noted that the interfacial layer obtained by the H_2O-based process is similar to that obtained by the $Hf(NEtMe)_4$ and H_2O[97] ALD process, but significantly thinner than in many other processes for HfO_2, *e.g.* $Hf(NMe_2)_4$ and H_2O,[105] $HfCl_4$ and H_2O,[70] or HfI_4 and O_2.[95] The 1 nm thick interfacial layer grown during the O_3-process is similar to that obtained with the $Hf(NEtMe)_4/O_3$ process on H-terminated Si.[48] However, it should be noted that thick interfacial layer obtained by the

ozone process will prevent obtaining very low CET values and thus the ozone-based processes may not be suitable for gate oxide deposition for MOSFETs but can have valuable impact on DRAM technology.

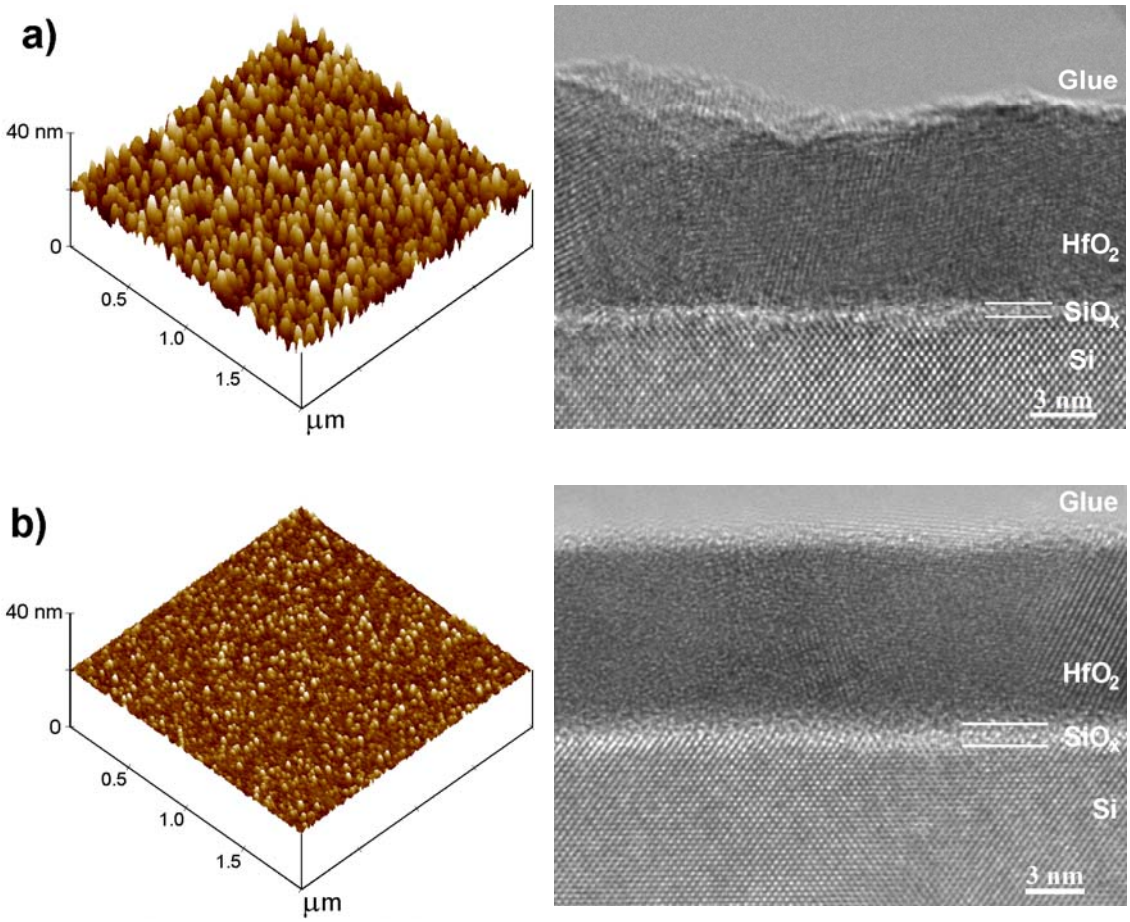

Figure 13. AFM and corresponding cross-sectional HR-TEM images of HfO_2 films deposited at 350°C on H-terminated Si(100) by (a) Cp_2HfMe_2/H_2O (500 cycles, HfO_2 thickness: 8.4-8.7 nm, rms-roughness: 1.8 nm) and (b) Cp_2HfMe_2/O_3 (200 cycles, HfO_2 thickness: 9.1 nm, rms-roughness: 0.4 nm) ALD processes. The interfacial layer thickness was 0.5 nm (a) and 0.9-1.1 nm (b). AFM image size: 2 x 2 μm^2.[V]

C-V curves for the capacitor structures, where the native oxide was removed prior to the deposition, are presented in Figure 14.[V] When water was used as an oxygen source, a rather stable *C-V* curve was observed. The V_{FB} shift and hysteresis were small and CET value of 4.1 nm was obtained for an 8.6 nm HfO_2 film. Similar dielectric properties but a slightly larger V_{FB} shift and a higher CET value, contributed by the thicker interfacial layer, were obtained for the ozone-processed film with 9.1 nm HfO_2 layer thickness. The

inset of Figure 14 illustrates the leakage current density *vs.* applied voltage curves for various Al/HfO_2/HF-etched/p-Si capacitor structures where HfO_2 was deposited with the ozone or water-based process. The island like nucleation in the water-processed films, lead to decreased density, as analyzed by XRR, which strongly affected the leakage current density values and breakdown voltages. The use of ozone has been reported to improve leakage current densities relative to water in ALD processes using $HfCl_4$[51] or $Hf(NMe_2)_4$[108,109] as the metal precursors. In the present case, more than an order of magnitude higher leakage current density values were obtained for the water-processed films than for the ozone-processed films. However, the thicker IL in the case of the ozone-processed film also contributed to the lower leakage current density. In addition, the breakdown voltage shifted to higher values when ozone was used.

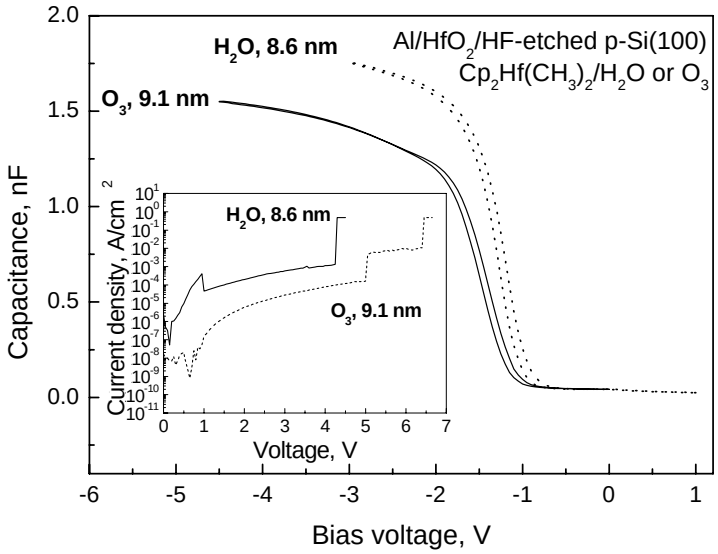

Figure 14. Capacitance-voltage curves of Al/HfO_2/p-Si structures grown at 350°C from $Cp_2Hf(CH_3)_2$ onto HF-etched substrate using ozone or water. Labels indicate the oxygen source used and the HfO_2 thickness measured. The inset depicts the leakage current density-voltage curves for these structures.[V] For Al/insulator/p-Si(100) structure the V_{FB} should be around –1.0 V.[155]

3.3 Rare earth oxide thin films from cyclopentadienyl precursors

3.3.1 Y_2O_3

ALD-type growth of Y_2O_3 was achieved with two precursor combinations, applying either Cp_3Y/H_2O or $(CpMe)_3Y/H_2O$ processes.[VI] ALD-type growth was confirmed in both processes at 250°C and 300°C. The growth rate obtained by the $(CpMe)_3Y/H_2O$ process was 1.2-1.3 Å/cycle in a wide temperature range, with the ALD window regime being 200-400°C. This growth rate is about six times higher than that obtained by the conventional $Y(thd)_3/O_3$ process.[135] The growth rate was further increased to 1.6 Å/cycle by using the Cp_3Y/H_2O process at 300°C, but an ALD window could not be detected with this precursor system. Generally, the Y_2O_3 films obtained with both Cp-based processes were stoichiometric and contained less than 0.5 at-% of carbon as an impurity. Hydrogen content was dependent on the deposition temperature being lowest at 0.9 at-% for the films deposited with the $(CpMe)_3Y/H_2O$ process at 400°C. Notably, the Y_2O_3 film crystallinity was strongly dependent on the precursor combination and the deposition temperature applied (Figure 15). The Cp_3Y as precursor yielded a significantly higher growth rate than $(CpMe)_3Y$ and in addition, the crystallinity of the Y_2O_3 films with the Cp_3Y/H_2O process was more pronounced, exhibiting (222) as the preferred orientation in the entire deposition temperature range of 175 to 400°C studied. In the case of the $(CpMe)_3Y$ precursor, more thermal energy was needed to achieve the (222) as the dominant orientation; the change from (400) to (222) as the preferred orientation occurs only around 400°C. When comparing the current Cp-based processes[VI] to the $Y(thd)_3/O_3$ ALD process,[135] the crystallinity was strongly enhanced (Figure 15). The increase in crystallinity as deposition temperature is increased also correlated with the surface morphology; both Cp-based processes the smoothest films were deposited at temperatures of 250°C or below.

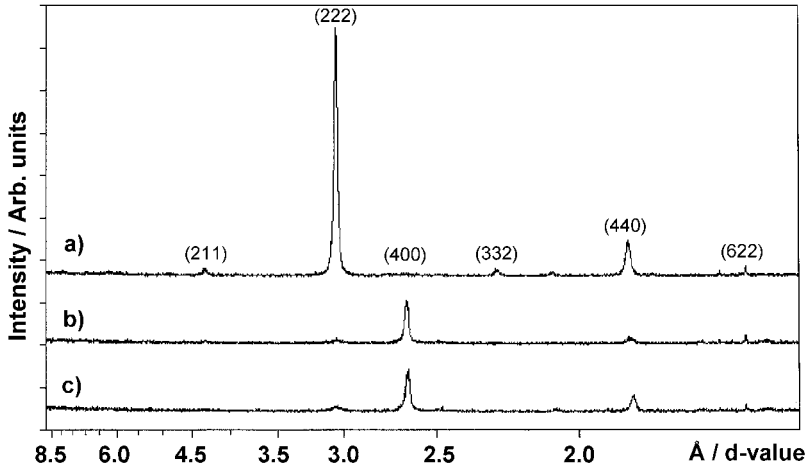

Figure 15. XRD patterns of Y_2O_3 films deposited at 250°C by the Cp_3Y/H_2O (a) and $(CpMe)_3Y/H_2O$ (b) processes. Y_2O_3 film thicknesses were 150 (a) and 125 nm (b).[VI] For comparison, an XRD pattern of a 125 nm thick Y_2O_3 film, deposited at 350°C by the $Y(thd)_3/O_3$ ALD process is presented (c).

3.3.2 LaO_x

In total, four different Cp-type precursors were tested with water as the oxygen source for the ALD of LaO_x. As seen in Table 6, where the results of ALD studies are summarized, the thermal stability of the applied La-precursors is limited. The Cp_3La decomposes at its sublimation temperature, excluding a self-limited growth mode. Introducing bulkier ligands, with methyl or isopropyl substitution on the Cp-ring, slightly improves the thermal stability and thereby uniform films on planar substrates could be obtained, but only at very low temperatures. However, it is obvious that partial decomposition lead to a CVD-type growth mode as lengthening of the precursor pulse also increased the growth rate and nonuniformity of the films. Because the ALD-type growth mode was not achieved, the experiments were not continued and detailed film characterization was omitted.

Table 6. Summary of ALD experiments carried out with various Cp-type La-precursors and water as the oxygen source. The standard La-precursor pulse length was 1.2 s.

La-precursor	Subl./evap. T at 2-3 mbar, °C		Deposition temperature tested, °C	Complete decomposition observed, °C	Growth rate (T), Å/cycle
Cp_3La	250	(solid)	260-300	>260	Dec.
$(CpMe)_3La$	165	(solid)	165-300	>170	2 (170°C)
$(CpMe_4)_3La$	175	(solid)	200	200	Dec.
$(Cp^iPr)_3La$	140	(liquid)	190-250	250	4.6 (190°C)

3.3.3 PrO_x

High-*k* PrO_x films have been successfully deposited by PVD methods[18] but employing ALD has been problematic.[144] Among the RE β-diketonates, $Pr(thd)_3$ used with ozone yielded nonuniform films, caused by the decomposition of the β-diketonate precursor.[138] Experiments with Cp_3Pr and water suffered from similar problems.[138] The thermal stability of the Cp-based precursor was improved through the use of an isopropyl substituent on the Cp ring. This resulted in high growth rate of about 1.6 Å/cycle at a deposition temperature of 175°C. The thickness uniformity over the 5 x 10 cm^2 substrate area was about 2 %. However, increasing the pulse length from 1.2 to 2.0 s resulted in films with a clearly higher growth rate (2.3 Å/cycle), and thus an ALD-type growth mode was not achieved. This is believed to have been caused by the partial decomposition of the $(Cp^iPr)_3Pr$ molecule in the gas phase or on the surface of the Si-substrate. At a still higher temperature of 225°C, precursor self-decomposition was evident as thickness nonuniformity was severe. Due to the insufficient thermal stability of the $(Cp^iPr)_3Pr$ precursor, a full characterization of the films was not performed.

3.3.4 Gd_2O_3

With $(CpMe)_3Gd$ and water in the temperature range of 175-300°C, ALD growth mode was not achieved (Figure 16).[VII] However, the thickness variation of the deposited films along the gas-flow direction was acceptable or less than 2 %. The growth rate of stoichiometric, polycrystalline Gd_2O_3 films was high, increasing from about 1.0 Å/cycle up to about 3.2 Å/cycle when growth temperature and pulse length were increased. In addition to the thickness variation also the impurity levels remained quite low, even below 1 at-% for C in the films deposited at 250°C. These characteristics indicate a low decomposition rate of the metal precursor.

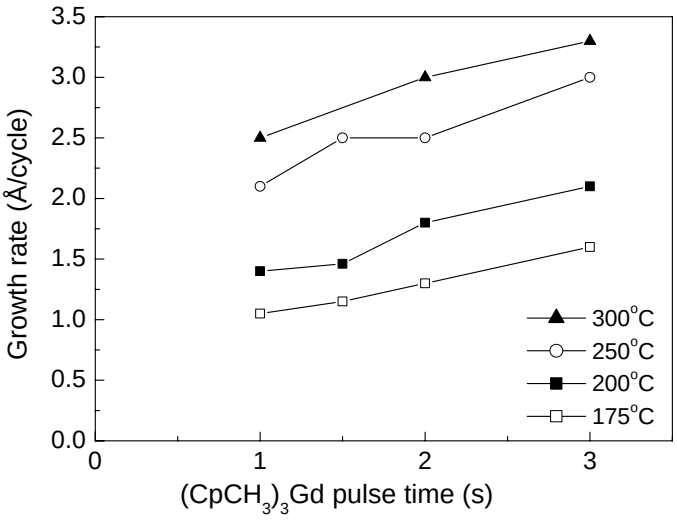

Figure 16. The growth rate of Gd_2O_3 films at different deposition temperatures plotted as a function of the $(CpMe)_3Gd$ precursor pulse length.[VII]

A comparison of the Gd_2O_3 films grown by the Cp-based process with the films obtained by the $Gd(thd)_3/O_3$ process reveals notable differences in growth characteristics. ALD-type growth was confirmed for the $Gd(thd)_3/O_3$ process, but the growth rate is significantly lower and the impurity levels higher than those obtained with the Cp-based process. Smoother films were obtained with the thd-based process (Figure 17), however.

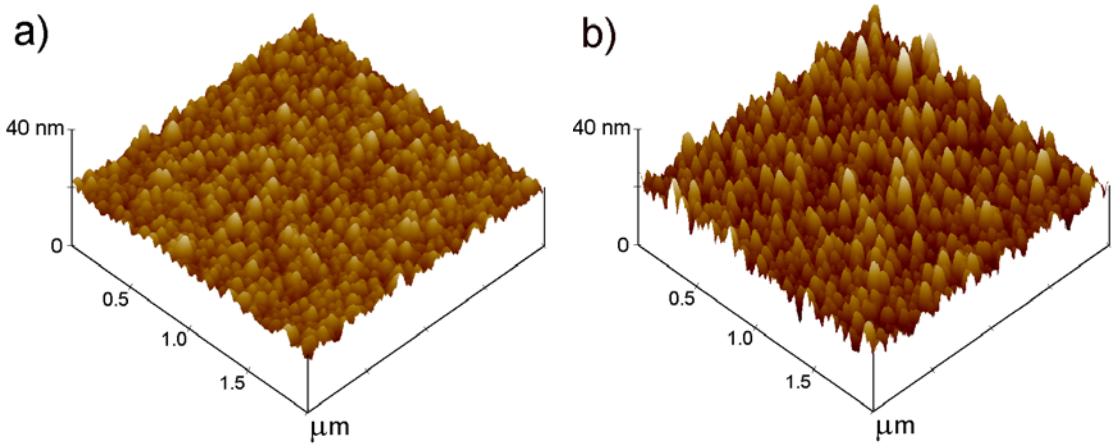

Figure 17. AFM images for 100 nm thick Gd_2O_3 films deposited at 250 °C by the $Gd(thd)_3/O_3$ (a) and $(CpCH_3)_3Gd/H_2O$ (b) processes. The rms-roughness values were 1.2 (a) and 2.5 nm (b), respectively.[VII]

While true ALD-type growth was not achieved by the $(CpMe)_3Gd/H_2O$ process, the more bulky $(CpMe_4)_3Gd$ precursor was tested in an attempt to overcome the partial decomposition problem. However, already at the deposition temperature of 250°C signs of precursor decomposition could be detected, and consequently the thickness uniformity was poor. Increasing the pulse length of the $(CpMe_4)_3Gd$ precursor from 1.2 s to 2.0 s enhanced the growth rate from 1.2 to 1.8 Å/cycle, which confirmed the absence of ALD-type growth mode.

3.3.5 Er_2O_3

A constant and high growth rate of 1.5 Å/cycle was achieved by the ALD process of Er_2O_3 employing $(CpMe)_3Er$ and H_2O as precursors at 250-350°C.[VIII] This well-behaving process yielded films with good uniformity and high purity. The impurity levels were lower than in the erbia films deposited by the thd- or amidinate-based processes.[42,136] The ALD-type growth mode was confirmed at 250 and 300°C where for complete saturation a pulse length of 1.5 s was required. The decomposition of the metal precursor affected the film growth behaviour at temperatures above 350°C. The rms-roughness increased as the deposition temperature was increased. The increase in crystallinity and, at temperatures above 350°C, the partial decomposition of the precursor is believed to cause the observed increase in roughness. Because of its thermal stability and reactivity, this Cp-precursor

offers clear advantages for Er_2O_3 film growth over the β-diketonate or amidinate-type erbium precursors.[42,136]

3.3.6 Rare earth scandates

Amorphous, high-permittivity rare earth scandates, namely $YScO_3$, $GdScO_3$ and $ErScO_3$, can be deposited by ALD using either Cp-type precursors and water or β-diketonate-type precursor and ozone as precursors.[IX,156] Considering that the ALD processes of the binary RE oxides are well-established and function in a self-controlled manner, RE scandates having a range of stoichiometries were straightforwardly deposited using different pulsing ratios in the RE processes, *e.g.* with pulsing ratio of 6:5 ($(CpMe)_3Y + H_2O$: $Cp_3Sc + H_2O$), a stoichiometry of $Y_{1.03}Sc_{0.96}O_{3.01}$ was achieved.[IX] By applying the same pulsing ratio but using $(CpMe)_3Er$ instead, the $Er_{1.02}Sc_{0.98}O_3$ composition was obtained. As expected, considerably higher growth rates were obtained with the Cp-based processes than with the β-diketonate-based processes. All the films were amorphous as deposited and crystallization upon annealing was dependent on the precursors used. The $YScO_3$ films deposited by the thd-precursors and ozone remained amorphous even after rapid thermal annealing at 800°C under N_2 ambient. In contrast, the $YScO_3$ films from the Cp-precursors became crystalline after RTA treatment at 800°C. It should be noted that the $YScO_3$ films crystallized as a solid solution of Y_2O_3 and Sc_2O_3 rather than forming a crystalline $YScO_3$ phase.[IX] In the case of $GdScO_3$ grown from thd-precursors and ozone, the Gd-scandate phase was observed to form after RTA treatment at 1000°C.[156] Stoichiometric $GdScO_3$ was deposited with a pulsing ratio of 5 : 11 ($Gd(thd)_3 + O_3$: $Sc(thd)_3 + O_3$).

3.3.7 Dielectric properties of the RE oxide films

Due to the thermal instability of the La- and Pr-precursors studied, thin La- or Pr-oxide layers for electrical measurements were not deposited. However, Al/RE oxide/native SiO_2/p- or n-Si/Al capacitor structures, where RE oxide layer was Y_2O_3, Gd_2O_3, Er_2O_3, $YScO_3$, $ErScO_3$, or $GdScO_3$, were measured for *C-V* and *I-V* characteristics. High positive fixed charges were detected in the Y_2O_3 films grown with both Cp-precursors.[VI] In addition, breakdown fields were rather low, likely caused by high crystallinity of the relatively thick films where the grain boundaries offer pathways for leakage current. Effective permittivity of the films was about 10, which is slightly lower than that obtained

with the Y[^{i}Pramd^{i}Pr]/H_2O ALD process.[146] It should be noted that annealing was not performed for these Y_2O_3 films,[VI] while in the study by de Rouffignac *et al.*[146] very long deposition times (>12 hrs for 50 nm film) were used, thus actually having an annealing effect during the deposition. Despite the fact that a true ALD-type growth mode was not achieved for the $(CpMe)_3Gd/H_2O$ process, the Gd_2O_3 films showed well-behaved *C-V* curves.[VII] The permittivity was in the range of 13-14, which is considerably higher than the values obtained for the Gd_2O_3 films grown by the thd-based process. However, flatband voltage shift, also reported for other RE oxides,[24] was significant. Similar to the case of Y_2O_3, leakage current was affected by the polycrystalline nature of the films.[VI,VII] Er_2O_3 films seemed to possess a reduced amount of fixed charge and their hysteresis was negligible.[VIII] The effective permittivity of a 12.5 nm Er_2O_3 film and native SiO_2 stack was about 10, but if the native SiO_2 interfacial layer is not taken into account, a value of 14 can be calculated for the erbia film.

The rare earth scandates, because of their amorphous structure seem to be better alternatives for gate dielectric applications than the more often studied RE binary oxides.[IX,156] Figure 18 depicts the *C-V* curves for capacitor structures where the insulator, $YScO_3$ or $GdScO_3$, is deposited by the thd-precursors and ozone. An effective permittivity of 14-15 could be calculated which is considerably higher than that (9-10) obtained for Y_2O_3, Gd_2O_3 and Sc_2O_3 binary oxides deposited from the thd-precursors. When Cp-precursors were applied for the deposition of $YScO_3$ and $ErScO_3$ the effective permittivity was high but considerable hysteresis was detected, indicating positively charged ions in the films. Because of the amorphous nature of the films, leakage current density remained low (*e.g.* 1 x 10^{-8} A cm^{-2} at $V=V_{FB}$ - 1 V for 40 nm $YScO_3$ film). Upon annealing at 1000°C, the crystallization as a solid solution of binary oxides leads to lower permittivity values as well as increased leakage current density. This pioneering study on ALD of RE scandates appears to offer an interesting starting point for further investigations aiming at high-*k* applications.

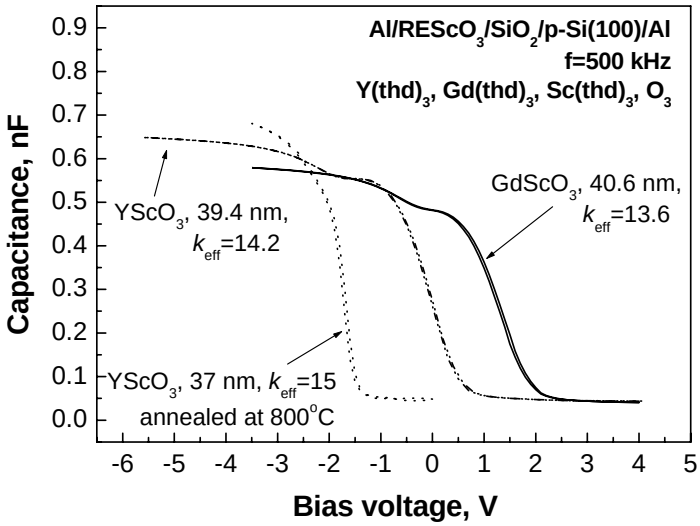

Figure 18. Capacitance-voltage curves of Al/$YScO_3$ or $GdScO_3$/native SiO_2/p-Si(100) capacitor structures with $YScO_3$ and $GdScO_3$ films deposited from Y(thd)$_3$ or Gd(thd)$_3$ and Sc(thd)$_3$ with O_3 as the oxygen source. Labels indicate the insulator thickness and effective permittivity values.[IX,156] For Al/insulator/p-Si(100) structure the V_{FB} should be around –1.0 V.[155]

3.3.8 Rare earth precursor selection

In the ALD of RE oxide thin films from Cp-type precursors, the limited thermal stability of the precursor seems to be the major problem. The correlation of the rare earth ionic radius and the ligand size on the thermal stability was previously introduced.[46] This prediction can now be complemented by the present results (Table 7). It clearly seems that introducing the bulkier Cp-ligands, *e.g.* with methyl or isopropyl substitution, thermal stability can be increased, but for large ions such as Pr^{3+} and La^{3+}, achievement of ALD-type growth mode at reasonable temperatures still remains a very challenging task.

Table 7. The suitability of different Cp-compounds applied/tested in the ALD processes for the growth of selected RE oxide films. Mixed-ligand compounds which contain Cp and some other ligands are omitted.

Rare earth	Ionic (+III) radius, Å	Ligand			
		Cp	**CpMe**	**Cp^{i}Pr**	**CpMe$_4$**
Sc	0.75	Suitable			
Er	0.89		Suitable		
Y	0.90	Suitable	Suitable		
Gd	0.94		Partial dec.		Partial dec.
Pr	0.99	Not suitable		Partial dec.	Not suitable
Ce	1.02		Not suitable		
La	1.03	Not suitable	Partial dec.	Partial dec.	Not suitable

4. CONCLUSIONS

The suitability of cyclopentadienyl-type precursors in ALD has earlier been established for noble metals,[157] alkaline-earth metal containing oxides[158,159] and sulfides[160] as well as for scandium oxide[133] deposition. For high-*k* oxide deposition the possibilities to modify the precursor chemistry are extensive. For the controlled ALD of ZrO_2 and HfO_2, the methyl-substituted Cp-type precursors, Cp_2ZrMe_2 and Cp_2HfMe_2, clearly have some advantageous features: The obtained film purity is high and the suitable deposition temperature is higher (up to 375-400°C) than in many other alternative halide-free processes. However, when water is used as the oxygen source the observed retarded growth on H-terminated Si can be considered as a drawback. With ozone, on the other hand, the roughness, impurity content, and leakage current density can be decreased. In general, the electrical characterization showed promising dielectric properties for high-*k* applications. The growth of ZrO_2 from Cp_2ZrMe_2 and deuterated water was studied *in situ* by QMS revealing that nearly all the methyl ligands and less than half of the Cp-ligands were released during the metal precursor pulse. The remaining ligands were released during the subsequent surface reaction with deuterated water, leaving the surface OD-terminated, and thus ready for the next cycle. The *in situ* studies showed that the decomposition onset temperature for Cp_2ZrMe_2 precursor was around 375°C.

A number of Cp-type precursors were applied for the deposition of RE oxides. Cp_3Y, $(CpMe)_3Y$, and $(CpMe)_3Er$ were found to have sufficient thermal stability in water-based processes for self-limiting, ALD-type growth of the corresponding RE oxide thin films. The growth rate was about six times higher than with the conventional β-diketonate precursors reacting with ozone.[24,135,VI,VIII] High purity, better stoichiometry as well as higher permittivity of the resulting oxide films can also be counted among the benefits of the current Cp-precursor approach. However, the thermal stability of the Cp-compounds is limited especially for larger RE ions, such as Gd, Pr and La. Stability can be improved by introducing bulkier ligands, such as isopropyl substitution, but in many cases partial decomposition destroys the preferred ALD-type growth mode resulting in films with poor uniformity. However, with the $(CpMe)_3Gd/H_2O$ process, high quality films on planar surfaces with promising dielectric properties were obtained despite the fact that partial decomposition prevented the surface-saturative growth mode.

Finally, ternary RE scandates, $YScO_3$, $GdScO_3$, and $ErScO_3$ were successfully grown by ALD as solid solutions of the individual binary oxides. These scandates were amorphous as-deposited and, depending on the precursor combination used, RTA at 800 or 1000°C was required for their crystallization. In addition to the amorphous structure, clearly beneficial to minimize leakage current, the effective permittivity (15-16) was considerably higher than that of the binary oxides (10).

The results obtained in this work show that Cp-type compounds are suitable for high-*k* depositions by ALD. Precursor chemistry is the key factor in the development of novel ALD processes and there Cp-type precursors offer a viable route to achieve high-quality oxide films not previously successfully processed by ALD. In addition, Cp-type precursors together with a proper oxygen source selection, can improve the film properties of important materials, such as ZrO_2 or HfO_2.

5. REFERENCES

1. Suntola, T. and Antson, J., *US Patent 4 058 430* (1977).
2. Leskelä, M. and Ritala, M., *Angew. Chem. Int. Ed.* **42** (2003) 5548.
3. *International Technology Roadmap for Semiconductors*, http://public.itrs.net/, 5.1.2006.
4. Hand, A. *Semicond. Int.* **26**(5) (2003) 46.
5. Wilk, G.D., Wallace R.M., and Anthony, J.M., *J. Appl. Phys.* **89** (2001) 5243.
6. Misra, D., Iwai, H., and Wong, H., *Electrochem. Soc. Interface* **14**(2) (2005) 30.
7. Robertson, J., *Rep. Prog. Phys.* **69** (2006) 327.
8. Houssa M. and Heyns, M.M., in *High-k Gate Dielectrics*, ed. Houssa, M., Institute of Physics Publishing, Bristol 2004, pp. 3-13.
9. Ritala M. and Leskelä, M., in *Handbook of Thin Film Materials*, ed. Nalwa, H.S., Academic Press, New York 2002, vol. 1, pp. 103-159.
10. Musgrave, C. and Gordon, R.G., *Future Fab. Int.* **18** (2005) 126.
11. Lysaght, P.S., Foran, B., Bersuker, G., Chen, P.J., Murto, R.W., and Huff, H.R., *Appl. Phys. Lett.* **82** (2003) 1266.
12. Niinistö, L., Päiväsaari, J., Niinistö, J., Putkonen M., and Nieminen, M., *Phys. Stat. Sol. A* **201** (2004) 1443.
13. Moore, G.E., *Electronics*, **38** (1965) 114.
14. http://www.intel.com, 4.1.2006.
15. Hubbard, K.J. and Schlom, D.G., *J. Mater. Res.* **11** (1996) 2757.
16. Schlom, D.G. and Haeni, J.H., *MRS Bull.* **27** (2002) 198.
17. Robertson, J., *Solid-State Electron.* **49** (2005) 283.
18. Osten, H.J., Bugiel, E., Kirfel, O., Czernohorsky, M., and Fissel, A., *J. Cryst. Growth* **278** (2005) 18.
19. Ribes, G., Mitard, J., Denais, M., Bruyere, S., Monsieur, F., Parthasarathy, C., Vincent, E., and Ghibaudo, G., *IEEE Trans. Device Mater. Reliab.* **5** (2005) 5.
20. Guha, S., Gusev, E., Copel, M., Ragnarsson, L.-Å., and Buchanan, *MRS Bull.* **27** (2002) 226.
21. Heeg, T., Wagner, M., Schubert, J., Buchal, C., Boese, M., Luysberg, M., Cicerrella E., and Freeouf, J.L., *Microelectron. Eng.* **80** (2005) 150.
22. Quevedo-Lopez, M.A., Krishnan, S.A., Kirsch, P.D., Pant, G., Gnade, B.E., and

Wallace, R.M., *Appl. Phys. Lett*. **87** (2005) 262902.

23. Osten, H.J., Bugiel, E., and Fissel, A., *Solid-State Electr*. **47** (2003) 2161.
24. Päiväsaari, J., Putkonen, M., and Niinistö, L., *Thin Solid Films* **472** (2005) 275.
25. Gerritsen, E., Emonet, N., Caillat, C., Jourdan, N., Piazza, M., Fraboulet, D., Boeck, B., Berthelot, A., Smith, S., and Mazoyer, P., *Solid-State Electron*. **49** (2005) 1767.
26. Pakkala, A., *AVS 4th International Conference on Atomic Layer Deposition*, Helsinki, Finland, 2004, Extended Abstracts on CD-ROM.
27. Niinistö, L., Ritala, M., and Leskelä, M., *Mater. Sci. Eng. B* **41** (1996) 23.
28. Leskelä, M. and Ritala, M., *Thin Solid Films* **409** (2002) 138.
29. Niinistö, L., *Curr. Opin. Solid State & Mater. Sci*. **3** (1998) 147.
30. Puurunen, R.L., *J. Appl. Phys*. **97** (2005) 121301.
31. Suntola, T., *Appl. Surf. Sci*. **100/101** (1996) 391.
32. Elers, K.-E., Blomberg, T., Peussa, M., Aitchison, B., Haukka, S., and Marcus, S., *Chem. Vap. Deposition* **12** (2006) 13.
33. Conley, Jr., J.F., Ono, Y., Zhuang, W., Tweet, D.J., Gao, W., Mohammed S.K., and Solanki, R., *Electrochem. Solid-State Lett.* **5** (2002) C57.
34. Matero, R., *Atomic Layer Deposition of Oxide Film–Growth Characterisation and Reaction Mechanism Studies*, Doctoral dissertation, University of Helsinki, Helsinki 2005, 61 p.
35. Jones, A.C., Aspinall, H.C., Chalker, P.R., Potter, R.J., Kukli, K., Rahtu, A., Ritala, M., and Leskelä, M., *J. Mater. Chem*. **14** (2004) 3101.
36. Jones, A.C., Aspinall, H.C., Chalker, P.R., Potter, R.J., Kukli, K., Rahtu, A., Ritala, M., and Leskelä M., *Mater. Sci. Eng. B* **118** (2005) 97.
37. Tiitta, M. and Niinistö, L., *Chem. Vap. Deposition* **3** (1997) 167.
38. *CVD on Nonmetals*, ed. Rees, Jr., W.S., VCH Verlagsgesellschaft GmbH, Weinheim 1996, 424 p.
39. Binnemans, K., in *Handbook on the Physics and Chemistry of Rare Earths*, eds. Gschneider, Jr., K.A., Bünzli, J.-C.G., and Pecharsky, V.K., Elsevier, Amsterdam 2005, Vol. 35, pp. 238-241.
40. Putkonen, M., *Development of Low-temperature Deposition Processes by Atomic Layer Epitaxy for Binary and Ternary Oxide Thin Films*, Doctoral dissertation, Helsinki University of Technology, Helsinki 2002, 69 p.
41. Lim, B.S., Rahtu, A., and Gordon, R.G., *Nature Mater.* **2** (2003) 729.

42. Päiväsaari, J., Dezelah, C.L., Back, D., El-Kaderi, H.M., Heeg, M.J., Putkonen, M., Niinistö, L., and Winter, C.H., *J. Mater. Chem.* **15** (2005) 4224.
43. Lujala, V., Skarp, J., Tammenmaa, M., and Suntola, T., *Appl. Surf. Sci.* **82-83** (1994) 34.
44. Kealy, T.J. and Pauson, P.L., *Nature* **168** (1951) 1039.
45. Miller, S.A., Tebboth, J.A., and Tremaine, J.F., *J. Chem. Soc*. (1952) 632.
46. Putkonen, M. and Niinistö, L., *Top. Organomet. Chem*. **9** (2005) 125.
47. Long, N.J., *Metallocenes: An Introduction to Sandwich Compounds*, Blackwell Science Ltd., Oxford 1998, 285 p.
48. Gusev, E.P., Cartier, E., Buchanan, D.A., Gribelyuk, M., Copel, M., Okorn-Schmidt, H., and D'Emic, C., *Microelectron. Eng*. **59** (2001) 341.
49. Park, C.S., Moumen, B.M., Sim, J.H., Barnett, J., Lee, B.H., and Bersuker, G., *Appl. Phys. Lett.* **87** (2005) 253510.
50. Ha, S.-C., Choi, E., Kim, S.-H., and Roh, J.S., *Thin Solid Films* **476** (2005) 252.
51. Park, H.B., Cho, M., Park, J., Lee, S.W., Hwang, C.S., Kim, J.-P., Lee, J.-H., Lee, N.-I., Lee H.-K., and Oh, S.-J., *J. Appl. Phys*. **94** (2003) 3641.
52. Copel, M., Gribelyuk M., and Gusev, E., *Appl. Phys. Lett.* **76** (2000) 436.
53. Green, M.L., Allen, A.J., Li, X., Wang, J., Ilavsky, J., Delabie, A., Puurunen, R.L., and Brijs, B., *Appl. Phys. Lett*. **88** (2006) 032907.
54. Nieminen, M., *Deposition of Binary and Ternary Oxide Thin Films of Trivalent Metals by Atomic Layer Epitaxy*, Doctoral dissertation, Helsinki University of Technology, Helsinki 2001, 57 p.
55. Ritala, M. and Leskelä, M. *Appl. Surf. Sci.* **1994**, 75, 333.
56. Perkins, C.M., Triplett, B.B., McIntyre, P.C., Saraswat, K.C., Haukka, S., and Tuominen, M., *Appl. Phys. Lett*. **78** (2001) 2357.
57. Kukli, K., Ritala, M., Aarik, J., Uustare T., and Leskelä, M. *J. Appl. Phys*. **92** (2002) 1833.
58. Aarik, J., Aidla, A., Mändar, H., Uustare T., and Sammelselg, V., *Thin Solid Films* **408** (2002) 97.
59. Sammelselg, V., Rauhala, E., Arstila, K., Zakharov, A., Aarik, J., Kikas, A., Karlis, J., Tarre, A., Seppälä, A., Asari, J., and Martinson, I., *Mikrochim. Acta* **139** (2002) 165.
60. Nohira, H., Tsai, W., Besling, W., Young, E., Petry, J., Conard, T., Vandervorst, W.,

De Gendt, S., Heyns, M., Maes, J., and Tuominen, M., *J. Non-Cryst. Solids* **303** (2002) 83.

61. Ferrari, S., Scarel, G., Wiernier, C., and Fanciulli, M., *J. Appl. Phys*. **92** (2002) 7675.
62. Zhao, C., Roebben, G., Bender, H., Young, E., Haukka, S., Houssa, M., Naili, M., De Gendt, S., Heyns, M., and Van Der Biest, O., *Microelectr. Reliability* **41** (2001) 995.
63. Besling, W.F.A., Young, E., Conard, T., Zhao, C., Carter, R., Vandervorst, W., Caymax, M., De Gendt, S., Heyns, M., Maes, J., Tuominen, M., and Haukka., S., *J. Non-Cryst. Sol.* **303** (2002) 123.
64. Rahtu, A. and Ritala, M., *J. Mater. Chem*. **12** (2002) 1484.
65. Conard, T., Vandervorst, W., Petry, J., Zhao, C., Besling, W., Nohira, H., and Richard, O., *Appl. Surf. Sci*. **203-204** (2003) 400.
66. Kukli, K., Forsgren, K., Ritala, M., Leskelä, M., Aarik, J., and Hårsta, A., *J. Electrochem. Soc.* **148** (2001) F227.
67. Kukli, K., Forsgren K., Aarik, J., Uustare, T., Aidla, A., Niskanen, A., Ritala M., Leskelä, M., and Hårsta, A., *J. Cryst. Growth* **231** (2001) 262.
68. Kukli, K., Ritala, M., Uustare, T., Aarik, J., Forsgren, K., Sajavaara, T., Leskelä, M., and Hårsta, A., *Thin Solid Films* **410** (2002) 53.
69. Forsgren, K., Westlinder, J., Lu, J., Olsson, J., and Hårsta, A., *Chem. Vap. Deposition* **8** (2002) 105.
70. Kukli, K., Ritala, M., Leskelä, M., Sajavaara, T., Keinonen, J., Gilmer, D.C., Hegde, R., Rai, R., and Prabhu, L., *J. Mater. Sci.; Mater. Electron*. **14** (2003) 361.
71. Hausmann, D.M., Kim, E., Becker J., and Gordon, R.G., *Chem. Mater*. **14** (2002) 4350.
72. Kim, Y., Koo, J., Han, J., Choi, S., Jeon, H., and Park, C.-G., *J. Appl. Phys*. **92** (2002) 5443.
73. Yun, S.J., Lim, J.W., and Lee, J.-H., *Electrochem. Solid-State Lett.* **7** (2004) F81.
74. Yun, S.J., Lim, J.W., and Lee, J.-H., *Electrochem. Solid-State Lett*. **8** (2005) F47.
75. Kim, J.Y., Kim, S.H., Seo, H., Kim, J.-H., and Jeon, H., *Electrochem. Solid-State Lett.* **8** (2005) G82.
76. Hausmann, D.M. and Gordon, R.G., *J. Cryst. Growth* **249** (2003) 251.
77. Nam, W.-H. and Rhee, S.-W., *Chem. Vap. Deposition* **10** (2004) 201.
78. Kukli, K., Ritala, M., and Leskelä, M., *Chem. Vap. Deposition* **6** (2000) 297.
79. Jeong, D., Lee, J., and Kim, J., *Integr. Ferroelect.* **67** (2004) 41.

80. Nakajima, A., Kidera, T., Ishii, H., and Yokoyama, S., *Appl. Phys. Lett*. **81** (2002) 2824.
81. Lao, S.X., Martin, R.M., and Chang, J.P., *J. Vac. Sci. Technol*. *A* **23** (2005) 488.
82. Endo, K. and Tatsumi, T., *Jpn. J. Appl. Phys*. **42** (2003) L685.
83. Matero, R., Ritala, M., Leskelä, M., Sajavaara, T., Jones, A.C., and Roberts, J.L., *Chem. Mater*. **16** (2004) 5630.
84. Matero, R., Ritala, M., Leskelä, M., Jones, A.C., Williams, P.A., Bickley, J.F., Steiner, A., Leedham, T.J., and Davies, H.O., *J. Non-Cryst. Solids* **303** (2002) 24.
85. Putkonen, M. and Niinistö, L., *J. Mater. Chem*. **11** (2001) 3141.
86. Yoshii, N., Takahashi, N., Nakamura, T., and Yoshioka, M., *Electrochem. Solid-State Lett.* **5** (2005) C85.
87. Kattelus, H., Ylilammi, M., Salmi, J., Aho, T.R., Nykänen, E, and Suni, I., *Mat. Res. Soc. Symp. Proc.*, **284** (1993) 511.
88. Ritala, M., Leskelä, M., Niinistö, L. Prohaska, T., Friedbacher, G., and Grasserbauer, M., *Thin Solid Films*, **250** (1994) 72.
89. Ganem, J.-J., Trimaille, I., Vickridge, I.C., Blin, D., and Martin, F., *Nucl. Instrum. Meth. Phys. Res. B*, **219-220** (2004) 856.
90. Gusev, E.P., Cabral, Jr., C., Copel, M., D'Emic, C., and Gribelyuk, M., *Microel. Eng*. **69** (2003) 145.
91. Aarik, J., Aidla, A., Kiisler, A.-A., Uustare T., and Sammelselg, V., *Thin Solid Films* **340** (1999) 110.
92. Aarik, J., Aidla, A., Mändar, H., Sammelselg V., and Uustare, T. *J. Cryst. Growth* **220** (2000) 105.
93. Triyoso, D.H., Hegde, P.I., White, Jr., B.E., and Tobin, P.J., *J. Appl. Phys*. **97** (2005) 124107.
94. Kukli, K., Ritala, M., Sajavaara, T., Keinonen J., and Leskelä, M., *Thin Solid Films* **416** (2002) 72.
95. Aarik, J., Sundqvist, J., Aidla, A., Lu, J., Sajavaara, T., Kukli, K., and Hårsta, A., *Thin Solid Films* **418** (2002) 69.
96. Kukli, K., Ritala, M., Sundqvist, J., Aarik, J., Lu, J., Sajavaara, T., Leskelä, M., and Hårsta, A., *J. Appl. Phys*. **92** (2002) 5698.
97. Kukli, K., Ritala, M., Lu, J., Hårsta, A., and Leskelä, M., *J. Electrochem. Soc.* **151** (2004) F189.

98. Kukli, K., Ritala, M., Leskelä, M., Sajavaara T., and Keinonen, J., *Chem. Vap. Deposition* **8** (2002) 199.
99. Kamiyama, S., Miura, T., and Nara, Y., *Appl. Phys. Lett.* **87** (2005) 132904
100. Ho, M.-T., Wang, Y., Brewer, R.T. Wielunski, L.S., Chabal, Y.J. Moumen, N., and Boleslawski, M., *Appl. Phys. Lett*. **87** (2005) 133103.
101. Liu, X., Ramanathan, S., Londergan, A., Srivastava, A., Lee, E., Seidel, T.E., Barton, J.T., Pang, D., and Gordon, R.G., *J. Electrochem. Soc*. **152** (2005) G213.
102. Senzaki, Y., Park, S., Chatham, H., Bartholomew, L., and Nieveen, W., *J. Vac. Sci. Technol. A* **22** (2004) 1175.
103. Kamiyama, S., Miura, T., and Nara, Y., *Electrochem. Solid-State Lett.* **8** (2005) F37.
104. Okuyama, Y., Barelli, C., Tousseau, C., Park, S., and Senzaki, Y., *J. Vac. Sci. Technol. A* **23** (2005) L1.
105. Kukli, K., Pilvi, T., Ritala, M., Sajavaara, T., Lu, J., and Leskelä, M., *Thin Solid Films* **491** (2005) 328.
106. Liu, X., Ramanathan S., and Seidel, T.E., *Mat. Res. Soc. Symp. Proc*. **765** (2003) 97.
107. Cho, M., Park, H.B., Park, J., Lee, S.W., Hwang, C.S., Jang G.H., and Jeong, J., *Appl. Phys. Lett*. **83** (2003) 5503.
108. Cho, M., Jeong, D.S., Park, J., Park, H.B., Lee, S.W., Park, T.J., Hwang, C.S., Jang, G.H., and Jeong, J., *Appl. Phys. Lett.* **85** (2004) 5953.
109. Park, J., Cho, M., Kim, S.K., Park, T.J., Lee, S.W. Hong, S.H., and Hwang, C.S., *Appl. Phys. Lett.* **86** (2005) 112907.
110. Deshpande, A., Inman, R., Jursich, G., and Takoudis, C., *J. Vac. Sci. Technol. A* **22** (2004) 2035.
111. Choi, S., Koo, J., Jeon, H., and Kim, Y., *J. Kor. Phys. Soc*. **44** (2004) 35.
112. Won, Y., Park, S., Koo, J., Kim, S., Kim, J., and Jeon, H., *Appl. Phys. Lett.* **87** (2005) 262901.
113. Kim, J., Kim, S., Jeon, H., Cho, M.-H., Chung, K.-B., and Bae, C., *Appl. Phys. Lett*. **87** (2005) 053108.
114. Kim, J., Kim, S., Kang, H., Choi, J., Jeon, H., Cho, M., Chung, K., Back, S., Yoo, K., and Bae, C., *J. Appl. Phys*. **98** (2005) 0945504.
115. Lee, S.-I., Owyang, J.S., Senzaki, Y., Helms, Jr., A., and Kapkin, K., *Solid State Technol*. **46** (2003) 45.
116. Lin, Y.-S., Puthenkovilakam R., and Chang, J. P., *Appl. Phys. Lett*. **81** (2002) 2041.

117. Kukli, K., Ritala, M., Leskelä, M., Sajavaara, T., Keinonen, J., Jones A.C., and Roberts, J.L., *Chem. Vap. Deposition* **9** (2003) 315.
118. Kukli, K., Ritala, M., Leskelä, M., Sajavaara, T., Keinonen, J., Jones, A.C., and Roberts, J.L., *Chem. Mater.* **15** (2003) 1722.
119. Kukli, K., Ritala, M., Leskelä, M., Sajavaara, T., Keinonen, J., Jones, A.C., and Tobin, N.L., *Chem. Vap. Deposition* **10** (2004) 91.
120. Conley, Jr., J.F., Ono, Y., Tweet, D.J., Zhuang W., and Solanki, R., *J. Appl. Phys*. **93** (2003) 712.
121. Takahashi, N., Nonobe, S., and Nakamura, T., *J. Sol. State Chem*. **177** (2004) 3944.
122. Conley, Jr., J.F., Ono, Y., Tweet D.J., and Solanki, R., *Appl. Phys. Lett*. **84** (2004) 398.
123. Gordon, R.G., Becker, J., Hausmann, D., and Suh, S., *Chem. Mater.* **13** (2001) 2463.
124. Nam, W.-H. and Rhee, S.-W., *Electrochem. Solid-State Lett*. **7** (2004) C55.
125. Park, H.B., Cho, M., Park, J., Lee, S.W., Park, T.J., and Hwang, C.S., *Electrochem. Solid-State Lett.* **7** (2004) G254.
126. Chang, H.S., Baek, S.-K., Park, H., Hwang, H., Oh, J.H., Shin, W.S., Yeo, J.H., Hwang, K.H., Nam, S.W., Lee, H.D., Song, C.L., Moon, D.W., and Cho, M.-H., *Electrochem. Solid-State Lett*. **7** (2004) F42.
127. Potter, R.J., Chalker, P.R., Manning, T.D., Aspinall, H.C., Loo, Y.F., Jones, A.C., Smith, L.M., Critchlow, G.W., and Schumacher, M. *Chem. Vap. Deposition* **11** (2005) 159.
128. Mölsä, H., Niinistö, L., and Utriainen, M., *Adv. Mater. Opt. Electron.* **4** (1994) 389.
129. Mölsä, H. and Niinistö, L., *Mater. Res. Soc. Symp. Ser*. **335** (1994) 341.
130. Päiväsaari, J., Niinistö, J., Myllymäki, P., Dezelah, C., Putkonen, M., Nieminen, M., Niinistö, L., and Winter, C.H., *Top. Appl. Phys*., in press.
131. Leskelä, M., Kukli, K., and Ritala, M., *J. All. Compd.*, in press.
132. Leskelä, M. and Ritala, M., *J. Solid State Chem.* **171** (2003) 170.
133. Putkonen, M., Nieminen, M., Niinistö, J., Niinistö, L., and Sajavaara, T., *Chem. Mater.* **13** (2001) 4701.
134. Nieminen, M., Putkonen, M., and Niinistö, L., *Appl. Surf. Sci.* **174** (2001) 155.
135. Putkonen M., Sajavaara T., Johansson L.-S., and Niinistö, L. *Chem. Vap. Deposition* **7** (2001) 44.
136. Päiväsaari, J., Putkonen, M., Sajavaara, T., and Niinistö, L., *J. All. Compd*. **374**

(2004) 124.

137. Kosola, A., Päiväsaari, J., Putkonen, M., and Niinistö L., *Thin Solid Films* **479** (2005) 152.
138. Päiväsaari, J., unpublished results.
139. Van, T.T. and Chang, J.P., *Appl. Surf. Sci.* **246** (2005) 250.
140. Van, T.T. and Chang, J.P., *Surf. Sci.* **596** (2005) 1.
141. He, W., Schuetz, S., Solanki, R., Belot, J., and McAndrew, J., *Electrochem. Solid-State Lett.* **7** (2004) G131.
142. Triyoso, D.H., Hegde, R.I., Grant, J., Fejes, P., Liu, R., Roan, D., Ramon, M., Wherho, D., Rai, R., La, L.B., Baker, J., Garza, C., Guenher, T., White, B.E., and Tobin, P.J., *J. Vac. Sci. Technol. B* **22** (2004) 2121.
143. Triyoso, D.H., Hegde, R.I., Grant, J.M., Schaeffer, J.K., Roan, D., White, B.E., and Tobin, P.J., *J. Vac. Sci. Technol. B* **23** (2005) 288.
144. Kukli, K., Ritala, M., Pilvi, T., Sajavaara, T., Leskelä, M., Jones, A.C., Aspinall, H.C., Gilmer D.C., and Tobin, P.J. *Chem. Mater.* **16** (2004) 5162.
145. Kukli, K., Ritala, M., Pore, V., Leskelä, M., Sajavaara, T., Hegde, R.I., Gilmer, D.C., Tobin, P.J., Jones, A.C., and Aspinall, H.C., *Chem. Vap. Deposition*, in press.
146. de Rouffignac, P., Park, J.-S., and Gordon, R.G., *Chem. Mater.* **17** (2005) 4808.
147. de Rouffignac, P.P. and Gordon, R.G., *AVS 5th International Conference on Atomic Layer Deposition*, San Jose, USA, 2005, Extended Abstracts on CD-ROM.
148. Gordon, R.G., *AVS 5th International Conference on Atomic Layer Deposition*, San Jose, USA, 2005, Extended Abstracts on CD-ROM.
149. Scarel G., Bonera E., Wiemer C., Tallarida G., Spiga S., Fanciulli M., Fedushkin I.L., Schumann H., Lebedinskii Y., and Zenkevich A., *Appl. Phys. Lett.* **85** (2004) 630.
150. Samuel, E. and Rausch, M.D., *J. Amer. Chem. Soc.* **95** (1973) 6263.
151. Eisentraut, K.J. and Sievers, R.E., *J. Amer. Chem. Soc.* **87** (1965) 5254.
152. Ylilammi, M. and Ranta-aho, T., *Thin Solid Films* **232** (1993) 56.
153. Putkonen, M., Sajavaara, T., Niinisto, L., and Keinonen, J., *Anal. Bioanal. Chem.* **382** (2005) 1791.
154. Rahtu A., *Atomic Layer Deposition of High Permittivity Oxides: Film Growth and In Situ Studies*, Doctoral dissertation, University of Helsinki, Helsinki 2002, p. 26.
155. Nicollian N.H. and Brews, J.R., *MOS (Metal Oxide Semiconductor) Physics and*

Technology, Wiley, New York 1982, p. 465.

156. Myllymäki, P., Niinistö, J., Putkonen, M., Nieminen, M., and Niinistö, L., *AVS 5th International Conference on Atomic Layer Deposition*, San Jose, USA, 2005, Extended Abstracts on CD-ROM.
157. Aaltonen, T., *Atomic Layer Deposition of Noble Metal Thin Films,* Doctoral dissertation, University of Helsinki, Helsinki 2005, 71 p.
158. Vehkamäki, M., Hatanpää, T., Hänninen, T., Ritala, M., and Leskelä, M., *Electrochem. Solid-State Lett*. **2** (1999) 504.
159. Putkonen, M., Sajavaara, T., and Niinistö, L., *J. Mater. Chem*. **10** (2000) 1857.
160. Ihanus, J., Hänninen, T., Hatanpää, T., Aaltonen, T., Mutikainen, I., Sajavaara, T., Keinonen, J., Ritala, M., and Leskelä, M., *Chem. Mater*. **14** (2002) 1937.